

1-1-2010

Dual Core Ytterbium Doped Fiber As A Gain Medium For A High Powered Swept Source Laser For Use In Multi-Channel Optical Coherence Tomography

Mark K. Harduar
Ryerson University

Follow this and additional works at: <http://digitalcommons.ryerson.ca/dissertations>



Part of the [Electrical and Electronics Commons](#)

Recommended Citation

Harduar, Mark K., "Dual Core Ytterbium Doped Fiber As A Gain Medium For A High Powered Swept Source Laser For Use In Multi-Channel Optical Coherence Tomography" (2010). *Theses and dissertations*. Paper 1383.

This Thesis is brought to you for free and open access by Digital Commons @ Ryerson. It has been accepted for inclusion in Theses and dissertations by an authorized administrator of Digital Commons @ Ryerson. For more information, please contact bcameron@ryerson.ca.

Dual Core Ytterbium Doped Fiber as a Gain Medium for a High Powered Swept Source Laser for Use in Multi-channel Optical Coherence Tomography

By

Mark Krishna Harduar, B.Eng

Ryerson University

Toronto, Ontario, Canada, 2008

A thesis

presented to Ryerson University

in partial fulfillment of the
requirements for the degree of

Master of Applied Science

in the program of

Electrical Engineering

Toronto, Ontario, Canada, 2010

© Mark Krishna Harduar 2010

Author's Declaration

I, Mark Krishna Harduar, declare that I am the sole author of this thesis.

I authorize Ryerson University to lend this thesis to other institutions or individuals for the purpose of scholarly research

Signature _____

I further authorize Ryerson University to reproduce this thesis by photocopying or by other means, in total or in part, at the request of other institutions or individuals for the purpose of scholarly research

Signature _____

Instructions to Borrowers

Ryerson University requires the signatures of all persons using or photocopying this thesis. Please sign below, and give the address and date.

Abstract

Dual Core Ytterbium Doped Fiber as a Gain Medium for a High Powered Swept Source Laser for use in Multi-channel Optical Coherence Tomography

Mark Krishna Harduar, Master of Applied Science, 2010

Department of Electrical and Computer Engineering, Program of Electrical Engineering,
Ryerson University

Optical coherence tomography (OCT) is a novel imaging modality that provides volumetric *in-vivo* high-resolution (1-15 μ m) images in real-time. Multi-channel OCT (MOCT) imaging utilizes many imaging channels simultaneously yielding several advantages over single-channel OCT. The benefits of MOCT are at the cost of the added requirement of several imaging beams, which demands high power output from the laser source. Dual-core Ytterbium (Yb) doped fiber was used in two configurations to demonstrate its use as a MOCT light source gain medium: 1) within a ring cavity resonator and 2) in a post-amplification regime with a low powered seed-laser. The amplification wavelength range was tailored to be centered at \sim 1060nm, where light absorption and scattering is at a minimum in water. In the post-amplification configuration, the output power was increased from 5mW to $>$ 200mW, with the axial resolution reducing from 10 μ m to 12 μ m. We also present initial *in-vivo* MOCT imaging of a tadpole.

Acknowledgements

I would like to thank my supervisor, Dr. Victor X.D. Yang. He has provided me with opportunities that I would never find in another lifetime. His hard work and dedication is an inspiration to everyone on our team. He has also remained a very cool supervisor and made my time as a graduate student very pleasurable.

Also, post doctorate fellow Dr. Beau A. Standish has provided invaluable amounts of mentorship and is a key contributor in my development as a researcher. Fellow masters student Michael Ka Kit Leung has helped me on many occasions with my work. From teaching me polygon alignment to point spread function measurement code, he always made himself available to help me despite his busy schedule. PhD candidate Adrian Mariampillia always showed enthusiasm towards his work, and especially towards this project. Adrian was the one who originated the work with the Ytterbium doped fiber as a gain medium and has given many suggestions and help with this project and others.

Dr. Xijia Gu is the most knowledgeable person I know when it comes to laser development and optics. He is directly responsible for teaching me the basics of optics in general through his optics course. He was also very generous with all of his equipment from his lab and his whole research lab was very easy to work with.

I would like to acknowledge all the others in the lab. Dr. Carry Sun, Ken (Masters) Lee, Timothy Luk, Benjamin Lee, Kyle Cheng, and Antonio Mauro have been easy to work with and have provided me with insightful discussions along the way. PhD

candidate Barry (Dr. Bear) Vuong, whom I've worked the most with in the lab, was always available at anytime for help with my work as well. Anna Farman and Karl (Frank Grimes) Magtibay helped during the tadpole imaging and they treated the tadpoles as one of their own children. Ahmad El-Falou and Patryk Skowron were also good summer students to work with as well.

Jenny Yeow has played a large role in our research lab. She has always been on top of the many components that I ordered for this project. Thanks for making everything in our lab run so smoothly. It was nice to have non-engineering discussions as well.

Dedications

This work is dedicated to my friends and family for their support and encouragement.

Table of Contents

1	Introduction.....	1
1.1	Objective.....	4
2	Background	6
2.1	Optical Coherence Tomography (Overview)	6
2.1.1	Interferometry	7
2.1.2	Transverse and Axial Resolutions.....	9
2.1.3	Fourier Domain OCT (FD-OCT).....	11
2.1.3.1	Spectral Domain OCT (SD-OCT).....	12
2.1.3.2	Swept Source OCT (SS-OCT)	13
2.1.4	Raster Scanning for Three-Dimensional OCT Imaging.....	13
3	Experimental Setup	15
3.1	Ytterbium (Yb).....	15
3.1.1	Yb Emission and Absorption	16
3.1.2	Dual Core Fiber	18
3.2	Laser Setup	19
3.2.1	Ring Cavities	19
3.2.1.1	Fourier Domain Mode Locking (FDML).....	23
3.2.1.2	Polygon Mirror Filter	24
3.2.2	Linear Cavity with Post Amplification.....	26
3.2.3	Imaging Optics / Electronics	27
4	Results.....	30

4.1	Amplified Spontaneous Emission Spectrums	30
4.2	Ytterbium’s Ability to Lase	31
4.2.1	Ring A.....	32
4.2.2	Ring B.....	33
4.2.3	Ring C.....	34
4.2.4	Ring D.....	35
4.3	Noise & Gain Figures, Polarization Extinction Ratio (PER)	36
4.4	Wavelength Sweeping Laser Source	37
4.4.1	Short Cavity.....	38
4.4.2	Long Cavity – FDML.....	39
4.5	Yb doped fiber in Post Amplification Configuration	40
4.5.1	20 Meters of Yb Doped Fiber.....	40
4.5.2	4 Meters of Yb Doped Fiber	41
4.5.2.1	Point Spread Function.....	42
4.5.2.2	Clock Signals	46
4.5.2.3	OCT Images.....	47
5	Discussion	50
5.1	Ring Configurations	50
5.2	Wavelength Sweeping Laser Source – Short	50
5.3	Wavelength Sweeping Laser Source – Long (FDML)	51
5.3.1	Chromatic Dispersion in Fibers.....	52
5.3.2	Dispersion in FDML Operation	52
5.3.3	Accepted Work Involving Yb Doped Fiber for a Swept Source Gain Medium	55
5.4	Post Amplification Configurations	64
5.4.1	Spectrums, Clock Signals, Point Spread Function.....	64

5.4.2	Image Analysis	65
6	Conclusion.....	68
6.1	Summary	68
6.2	Future Work.....	71
6.3	Impact to the Field	74
7	Bibliography	75

List of Tables

Table 1: Summary of 3 Yb-doped fiber lengths.....	30
Table 2: Summary of the point spread function measurement.....	45

List of Figures

Figure 1-1: Comparison of image resolution and penetration of US, OCT & confocal microscopy [2].....	2
Figure 1-2: Light absorption and scattering in water [10].....	4
Figure 2-1: Michelson interferometer, interference of long and short coherence light [2]	8
Figure 2-2: OCT setup [13] and an OCT image of fingernail [14].....	9
Figure 2-3: Trade-off between transverse resolution and depth of focus.....	10
Figure 3-1: Transitions of energy levels during fluorescents	16
Figure 3-2: The absorption (solid) and emission (dotted) Spectrums of Yb Doped Fiber [16]	17
Figure 3-3: Ring cavities (A and B) setups to test the dual core Yb doped fiber as a gain medium	21
Figure 3-4: Ring cavities (C and D) setups to test the dual core Yb doped fiber as a gain medium	22
Figure 3-5: Wavelength sweeping ring cavity laser	22
Figure 3-6: Polygon filter configuration, conceptual (left), actual (right)	26
Figure 3-7: Linear cavity using Yb doped fiber as post amplifier	26
Figure 3-8: System diagram of imaging optics	28
Figure 4-1: Amplified spontaneous emission of various Yb doped fiber lengths	30
Figure 4-2: Amplifies spontaneous emission of a 915nm and a 976nm pump.....	31
Figure 4-3: Linewidth of the filter	32
Figure 4-4: Lasing of different wavelengths in the Ring A configuration.....	33

Figure 4-5: Gain of different wavelengths in the Ring A configuration.....	33
Figure 4-6: Lasing of different wavelengths in the Ring B configuration.....	34
Figure 4-7: Gain of different wavelengths in the Ring B configuration.....	34
Figure 4-8: Lasing of different wavelengths in the Ring 3 configuration.....	35
Figure 4-9: Gain of different wavelengths in the Ring 3 configuration.....	35
Figure 4-10: Lasing of different wavelengths in the Ring D configuration.....	36
Figure 4-11: Lasing of different wavelengths in the Ring D configuration.....	36
Figure 4-12: Gain and noise measurement data.....	37
Figure 4-13: Lasing bandwidth seen from the Yb-doped fiber.....	38
Figure 4-14: Output spectrum using 4m of Yb doped fiber in a short cavity	39
Figure 4-15: Output spectrum in FDML operation at 3 different sweeping frequencies..	40
Figure 4-16: SS-OCT seed laser spectrum before and after 20 m of Yb doped fiber	41
Figure 4-17: SS-OCT seed laser spectrum before and after 4m of Yb doped fiber	42
Figure 4-18: Interferometer setup for point spread function.....	43
Figure 4-19: Point spread function measurement of the seed laser	43
Figure 4-20: Point spread function measurement of the seed laser and Yb doped fiber without pumping.....	44
Figure 4-21: Point spread function measurement of the seed laser and Yb doped fiber with pumping.....	44
Figure 4-22: Clock signal of the laser source pre and post amp.....	46
Figure 4-23: A 1-channel <i>in vivo</i> image (pre-amp) of a tadpole heart	47
Figure 4-24: A 2-channel <i>in vivo</i> image (pre-amp) of a tadpole heart	48
Figure 4-25: A 2-channel <i>in vivo</i> image (post-amp) of a tadpole heart.....	49

Figure 5-1: Dispersion curves for HI1060 and SMF-28 fibers	54
Figure 5-2: Simple structure detector algorithm.....	66
Figure 5-3: Structural image of channel A of MOCT image pre (left) and post (right) amplification	66
Figure 5-4: Structural detection of channel A of MOCT Imaging for pre (left) and post (right) amplification.	67
Figure 6-1: Suggested cavity design for an improved spectral FDML response.....	73

1 Introduction

Medical imaging techniques are important in any field of medicine as they assist with the diagnosis and clinical management of many onset diseases that patients may suffer from. Minimally invasive imaging techniques have been essential in diagnostic medicine over the last half-century. X-ray computed tomography (CT), magnetic resonance imaging (MRI), functional magnetic resonance imaging (fMRI), positron emission tomography (PET), single-photon emission computed tomography (SPECT) and Ultrasound (US) are all well developed and widely accepted as standard 3-dimensional imaging modalities. However, the spatial resolutions of these technologies are all limited to a few millimeters [1]. An imaging modality that has a higher-resolution, in the sub-micron range, is confocal microscopy, however the image penetration is limited to only a few hundred micrometers. Optical coherence tomography (OCT), a relatively new imaging technique, can achieve axial resolutions between 1 – 15 μ m and a penetration depth that is limited to 2 – 3 mm. In terms of imaging depth and resolution, OCT's performance is complimentary to the coarser imaging modalities (US, CT, MRI, etc) and to the finer imaging modalities (confocal microscopy) [2] as it allows for higher resolution while maintaining a depth of field. Figure 1-1 demonstrates how confocal microscopy, OCT and US are all complimentary to one another based on image resolution and image penetration. Without OCT, there would exist a gap in imaging modalities in terms of resolution and depth.

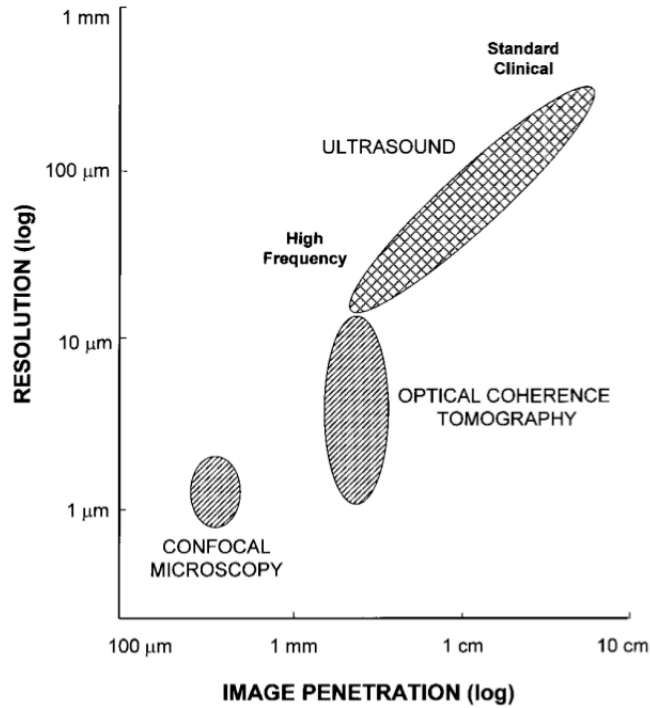


Figure 1-1: Comparison of image resolution and penetration of US, OCT & confocal microscopy [2]

Currently, the largest clinical application of OCT is in ophthalmology, within the eye, where it has been proven to provide information on retinal pathology, and ultrahigh-resolution OCT has been proven to provide information on the intra-retinal properties [3]. However OCT's applications extend to other fields of medicine outside of the ophthalmology, one of which includes endoscopic imaging [4] [5] [6], where small optics are utilized for cathertization of image probes to image from within. OCT has also been proven to help with *in vivo* pathology and catheter navigation in both the cardiovascular system and the gastrointestinal tract [7] [8].

Multichannel OCT (MOCT) has previously demonstrated several unique advantages in OCT imaging where multiple light beams are used to image a single sample in parallel. MOCT can then be used to increase the transverse (or lateral) resolution of the imaging by implementing multiple beams with a high numerical

aperture (NA) lens and have the light focused at several different depths of the tissue. MOCT has previously demonstrated uses in endoscopic imaging [5] while other advantages include faster image acquisition rates without an increase in swept-source laser speed and without increasing the detector bandwidth speed. Faster imaging speed also helps to further reduce image artifacts on *in vivo* subjects, such as bulk tissue motion [9]. In Doppler OCT, blood flow quantifications are made based on the phase change of the backscattered wave. With MOCT, because high scan rates are possible without an increasing the axial-scan rate of the source laser, the blood flow sensitivity is not compromised by the increase in image acquisition speed. Relatively slower axial-scan rates are important in Doppler OCT as it allows for a larger phase built up time of the back reflected waves when detecting slow flow rates resulting in the higher sensitivity Doppler measurement. To implement a MOCT system, the light source is split into several channels while the total output power per channel is reduced causing a degradation in the signal to noise ratio.

In conventional OCT, the wavelengths that are utilized are either 1310nm or 800nm, which are based on the equipment that was originally designed for communications in fiber optics. Many have considered OCT light sources with a wavelength centered at 1060nm based on the optical properties of water. A significant portion of biological tissue is made of up water, and this makes it important to know the absorption and scattering of light in water as a function of wavelength. The absorption and scattering minimums have been previously demonstrated [10]. The absorption and scattering of broadband light in water occurs in this fashion based on the molecular structure of H₂O.

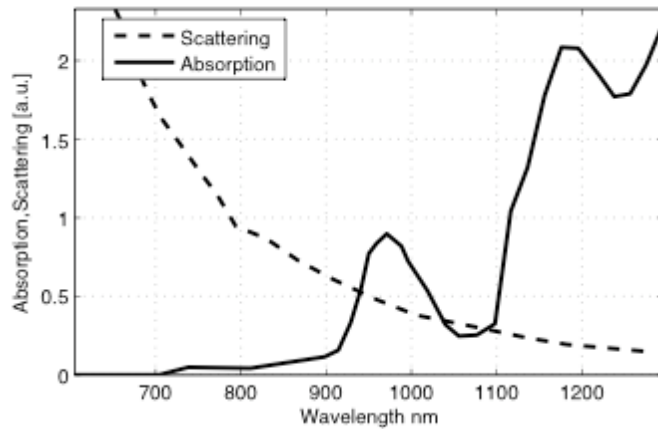


Figure 1-2: Light absorption and scattering in water [10]

Figure 1-2 demonstrates the light scattering of water in the dashed line and the light absorption of water is in solid black. At 1060nm there is an ideal trade off between the absorption and scattering spectras. With a 1060nm light source, deeper light penetration is possible as it further extends the visible depth window, compared to typical 1310nm and 800nm light sources in watery tissue [11].

1.1 Objective

The objective of this thesis was to create an OCT light source system that can make use of several channels for MOCT imaging while also having a center wavelength at 1060nm to take advantage of the light absorption and scattering minimum. Firstly a large enough output power to support several channels is needed and secondly to have a large enough bandwidth centered at 1060nm to provide an axial resolution that is comparable to other 1060nm light sources. This project had to have yielded an OCT system with the highest documented optical output power and for the first time, demonstrate a multi-channelled OCT system in the 1060nm range. This project needed to be a direct replacement for multi-channelled laser sources, which currently uses a multiple SOA

design [9]. A through design process for the high powered laser needed to be outlined and its characteristics such as lasing and saturation needed to be well documented. The laser source needed to be completely comprised of 1060nm components for optimal imaging. A gain medium of Ytterbium (Yb) was used to achieve the required high optical power. A methodology of designing a specific emission spectrum of Yb is also presented here. The Yb gain medium was to be used to make both a swept source laser and a post amplifier for an SOA based seed laser. To prove this laser's ability as an OCT source, imaging was performed on a *Xenopus Laevis* tadpole.

2 Background

2.1 Optical Coherence Tomography (Overview)

Optical coherence tomography (OCT) is analogous to Ultrasound (US) in the fact that a wave propagates and interrogates the sample tissue and images are produced based on the backscattered and or back-reflected waves. However, in OCT, light waves are utilized as apposed to sound waves, direct contact between the wave source and the imaged sample is not necessary. The wavelengths often used in OCT ($\sim 1.3\mu\text{m}$) are much shorter than those of ultrasound ($>50\mu\text{m}$) allowing for a higher spatial resolution. However, the trade off of OCT's excellent resolution comes at the cost of penetration, which is limited to 1-3mm due to optical scattering. The major difference between OCT and US is the speed of the propagating wave. The velocity of sound waves in water is $\sim 1.5 \times 10^3 \text{ m/s}$ which is a slow enough speed for modern electronics to construct images based on the time delay of the backscatter or backreflected waves. However, the velocity of light is $\sim 3 \times 10^8 \text{ m/s}$, which is orders of magnitudes higher than that of sound and there are no existing electronic solutions to support the direct measurements for the time-delay of backscattered light. For example, if the time delay measurement of light were used for a structural image with a resolution in the $10\mu\text{m}$ scale, this would correspond to a time resolution of 30 fs [2]. To over come this issue, correlation or interferometry techniques are employed [12] to gate the data acquisition and produce depth resolved reflectivity measurements of the sample of interest. The principals of interferometry are discussed in more detail in following section.

2.1.1 Interferometry

Interferometry is a fundamental component in all OCT systems, which allows for measurement of the backscattered wave without measuring the direct time of flight difference of the light. Figure 2-1 shows a Michelson interferometer setup in its simplest form. The light that is emitted from the source can be represented by $E_i(t) = E_i \cos(\omega t - kz)$, where E_i is the electric field at position z at time t . k is the wave number given by $2\pi/\lambda$, where λ is the wavelength and ω is the angular frequency. The light is divided into two paths by a beam-splitter (BS). One path goes to a reference mirror while the other path goes to a sample, whose light will be denoted as $E_r(t)$ and $E_s(t)$ respectively. After reflection, the beams travel back to the beam-splitter and are recombined together. The output of the interferometer seen at the detector is $\sim E_r(t) + E_s(t)$. The detector measures the intensity of the output beam, which is proportional to the square of the electromagnetic field. If the distance traveled in the reference and sample lengths are represented by l_r and l_s respectively, the intensity seen at the detector is:

$$I_0(t) \sim \frac{1}{4}|E_r|^2 + \frac{1}{4}|E_s|^2 + \frac{1}{2}E_r E_s \cos\left(2\frac{2\pi}{\lambda}\Delta l\right) \quad \text{Eq. 2-1}$$

Where Δl is the path difference between l_r and l_s . From Eq. 2-1, it can be seen that as the path difference varies, the output intensity will oscillate. The bottom of Figure 2-1 shows the detected signal, $I_o(t)$ from the interference of a light source with a long coherence length (monochromatic) and the signal from a short coherence length (broad band). The coherence length is inversely proportional to the bandwidth of light. When a low coherence light source is used, interference is only observed when the reference and sample arms are matched within the coherence length [2].

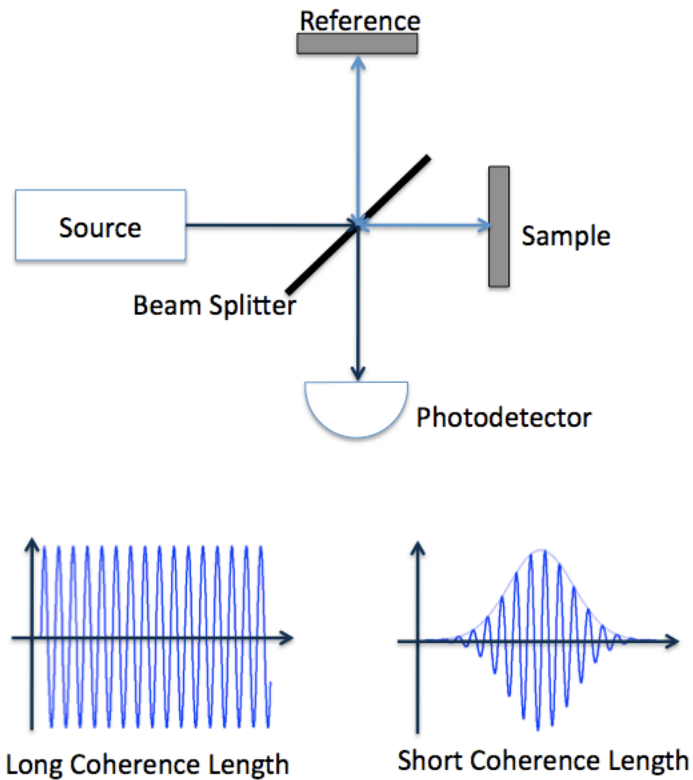


Figure 2-1: Michelson interferometer, interference of long and short coherence light [2]

Figure 2-2 depicts the setup of a Michelson interferometer for use as an OCT system. A fibre-coupler is used instead of a free space beam splitter. The reference mirror can be translated back and forth for an OCT depth scan. Three-dimensional imaging is achieved by a scanning mirror and a focusing lens that is directing the light onto the sample in a raster scanning fashion. The setup shown is known as a time domain OCT (TD-OCT) system. More recent OCT systems take advantage of a frequency domain setup where translated mirror is eliminated.

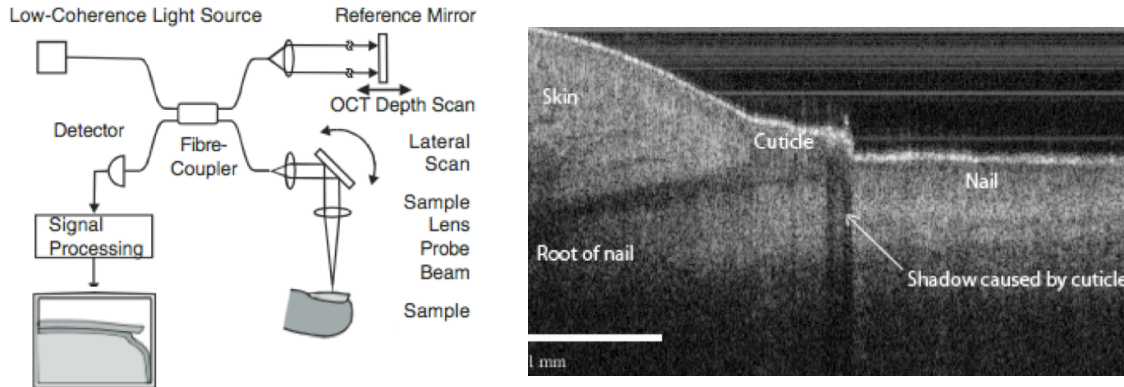


Figure 2-2: OCT setup [13] and an OCT image of fingernail [14]

Aside from interferometry, another difference between OCT and Ultrasound is the governing factors of image resolution.

2.1.2 Transverse and Axial Resolutions

In OCT, the resolutions of the systems are important specifications to indicate the quality of the image. Unlike many other imaging modalities, such as Ultrasound, the axial and transverse resolutions are independent of one another. The transverse resolution (lateral) is dependant on the imaging optics in the sample arm, such as the focusing lens. Given a specific lens, the minimum spot size (Δx) that the sample beam can be focused is given by the equation:

$$\Delta x = \frac{4\lambda}{\pi} \left(\frac{f}{d} \right) \quad \text{Eq. 2-2}$$

Where d is the spot size of the incident beam on the lens and f is the focal length of the lens. Very high transverse resolution can be achieved by using a lens with a high numerical aperture (NA) however this will reduce the depth of focus (b) which changes as a function of the spot size from the following equation:

$$b = \frac{\pi \Delta x^2}{2\lambda} \quad \text{Eq. 2-3}$$

Figure 2-3 visually depicts the trade-off between the spot size of the beam and the depth of focus [2]. If a high-resolution narrow Δx is desired the range in depth is reduced. One advantage that MOCT has previously shown, was if multiple imaging beams with high NA are sequentially placed at several different depths (separated by a distance of b) the overall transverse resolution is increased.

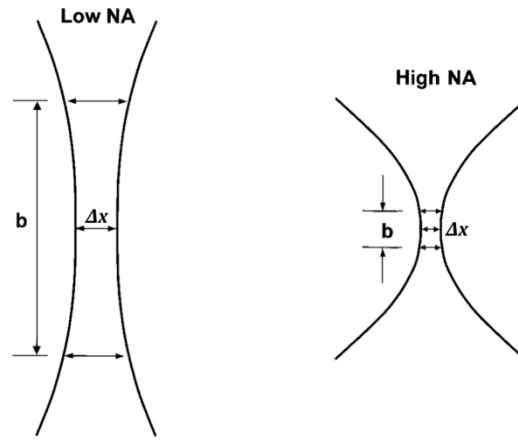


Figure 2-3: Trade-off between transverse resolution and depth of focus

The coherence length of the light source determines the axial resolution, which is independent of the focusing optics. The expected axial resolution of a light source can be calculated with the following formula:

$$\Delta z = 2 \ln(2) \frac{\lambda_c}{\pi \Delta \lambda} \quad \text{Eq. 2-4}$$

Where λ_c is the center wavelength of the broadband light source and $\Delta \lambda$ is the bandwidth of the light source at full-width half-maximum (FWHM). For better resolution images,

shorter wavelengths and a wider bandwidth should be used [1]. Eq. 2-4 is an important parameter in light source design as it is an indicator of the achievable axial resolution.

2.1.3 Fourier Domain OCT (FD-OCT)

In Fourier domain (FD) OCT imaging the translating reference mirror used for depth scanning has been replaced by either a wavelength tuning light source or a CCD (charged-couple device) camera for either swept source OCT or spectral domain OCT, respectively. As FD-OCT does not require a translating reference mirror, the image acquisition speed can be increased substantially. The method for resolving depth without a translating mirror is described below.

Let the backscattered light from the sample be represented by U with different depths, z :

$$U(z) = U_0 e^{-ik_0 n z} \quad U_z = U_0 e^{-ik_0 n z}$$

Where U_0 is the amplitude, $k_0 = 2\pi/\lambda_0$ is the wave number, λ_0 is the wavelength, n is the index of refraction.

If the light source was comprised of single monochromatic light, the interference seen by the photodetector can be represented by $I_{\Delta z}(k_0)$:

$$\begin{aligned} I_{\Delta z}(k_0) &= |(U_r + U_s)|^2 \\ I_{\Delta z}(k_0) &= \left| U_0 \left(e^{-ik_0 n z} + e^{-ik_0 n (z+2\Delta z)} \right) \right|^2 \\ I_{\Delta z}(k_0) &= U_0^2 \left(e^{-ik_0 n z} + e^{-ik_0 n (z+2\Delta z)} \right) \left(e^{ik_0 n z} + e^{ik_0 n (z+2\Delta z)} \right) \\ I_{\Delta z}(k_0) &= U_0^2 \left(2 + e^{ik_0 n 2\Delta z} + e^{-ik_0 n 2\Delta z} \right) \\ I_{\Delta z}(k_0) &= U_0^2 \left(1 + \cos(k_0 2\Delta z) \right) \end{aligned} \quad \text{Eq. 2-5}$$

Where U_r and U_s represent the light from reference and sample arms respectively which

are equal in magnitude. $2\Delta z$ represents the path difference that the light travels between the two arms. The reflectivity of the imaged sample is depth dependent, let $a(z)$ represent that reflectivity profile at any given beam position then U_r can be replaced by $U_o a(z)$.

Given this, the intensity from many different depths can be summarized as:

$$I(k_0) = 2I_0 \left(1 + \int_0^{\infty} a(z) \cos(2k_0 n z) dz \right)$$

If a broadband light source is used instead of a monochromatic light the interference signal can be represented by:

$$I(k) = 2I_0 \left(1 + \int_0^{\infty} a(z) \cos(2knz) dz \right)$$

It can now be seen that the depth information is encoded in the cosine argument. By definition of the Fourier transform, an intensity profile based on depth can be resolved:

$$I(z) = FT \left\{ 2I_0 \left(1 + \int_0^{\infty} a(z) \cos(2k_0 n z) dz \right) \right\} \quad \text{Eq. 2-6}$$

2.1.3.1 Spectral Domain OCT (SD-OCT)

In Spectral Domain OCT, a wide bandwidth super-luminescent diode (SLD) is utilized as the light source. The light source interrogates the tissue after it passes through an interferometer similar to one described in Figure 2-2. Instead of the interference signal being read by a high-speed detector, the light is collimated onto a high-density groove grating and onto a high-speed CCD detector array. This configuration separates the

wavelengths so the spectrum of the interference can be determined. After a Fourier transform, the depth profile can be deciphered. Although a large improvement over TD-OCT is seen, the high-speed CCD detector array is still seen as limiting factor due to the discharge time in an individual CCD detector and is slow in comparison to swept-source OCT (SS-OCT).

2.1.3.2 Swept Source OCT (SS-OCT)

With swept source OCT, the laser source is made up of a small filtered linewidth ($\Delta\lambda$), which is swept linearly in wavelength over time. The entire sweep range is considered as the spectral width. A high-speed photodetector is used as apposed to a CCD detector array. The combination of a high-speed photodetector and a wavelength-sweeping source creates a time resolved spectrometer. As a photodetector only registers photons, regardless of the wavelength, it has a reduced data acquisition time compared to CCD detector's relative longer discharge time. During imaging with an SS-OCT each wavelength sweep through the entire spectral bandwidth corresponds to a single axial scan.

2.1.4 Raster Scanning for Three-Dimensional OCT Imaging

The aforementioned sections describe OCT imaging along a one-dimensional axis (axial-scan). To achieve a full three-dimensional volumetric OCT image, the imaging beam needs to be translated laterally to a different position. After successive axial scans the imaging beam is swept in a single direction to create a two-dimensional (b-mode) image. Obtaining successive b-mode images at different positions a three-dimensional OCT image is constructed through a raster scanner

mechanism. There are several implementations to achieve volumetric imaging though the use of small-catheterized MEMS devices [6] or through physically rotating the sample arm [14].

3 Experimental Setup

All experimental setups use a dual core Yb doped fiber as the gain medium.

Three main regimes for amplification were tested: a short cavity, a long cavity and post amplifier. Several configurations were tested for each of the three regimes.

3.1 Ytterbium (Yb)

Ytterbium (Yb^{3+}) ion, atomic number 70, is a rare-earth metal used as a dopant in many fiber-lasers (YDFAs). The purpose of using Yb for OCT imaging is directly related to its fluorescence spectrum. To understand the concept of fluorescence, the rare-earth metal must be looked at on an atomic level. The ground state of this atom has a given energy E_1 . When the atoms absorb an energy in the form of light, with a frequency ν_{31} , its electrons are excited to a higher energy level, E_3 . The elevation of the atom's energy can be calculated as: $E_3 - E_1 = h\nu_{31}$, where h is Planck's constant. This process is known as pumping, as shown in Figure 3-1(P). The next transition (R) is the one from E_3 down to E_2 . In order for the energy level to be dropped to E_2 , energy is released in a radiationless form, usually emitted as vibrational motion. The transition (L) from E_2 to E_1 is a longer process and this energy is released as a photon. The photon that is released can be calculated as $E_2 - E_1 = h\nu_{21}$, where ν_{21} is the frequency of the emitted photon [15].

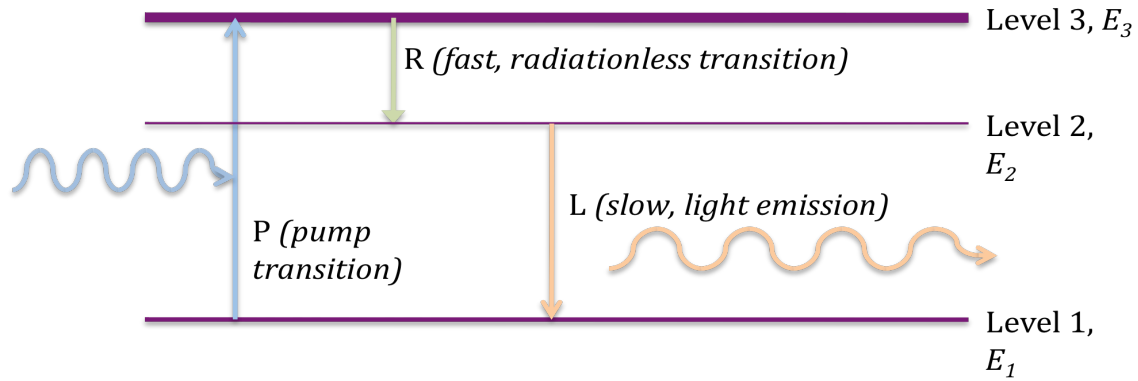


Figure 3-1: Transitions of energy levels during fluorescents

Because frequency and wavelength are inversely proportional, when the smaller $h\nu_{21}$ energy is emitted, it is emitted as a longer wavelength. In the case of Yb, the ground state manifold of the atom is $^2F_{7/2}$ while the excited state manifold is at $^2F_{5/2}$.

3.1.1 Yb Emission and Absorption

The cross-sectional absorption and spontaneous emission spectrums of Yb have previously been demonstrated [16]. The absorption spectrum in Figure 3-2 (left, solid) was obtained by fully saturating a given length of Yb doped fiber with white light and observing the un-absorbed light. Re-absorption is when a photon is initially absorbed and emitted as a longer wavelength and this longer wavelength itself is absorbed again and emitted as a successively longer wavelength. To avoid complications of re-absorption when monitoring the spontaneous emission, the measurement was taken along the side of the fiber as apposed to the fiber end. The assumption was made that the peak of the absorption spectrum was equal to the peak of the emission spectrum.

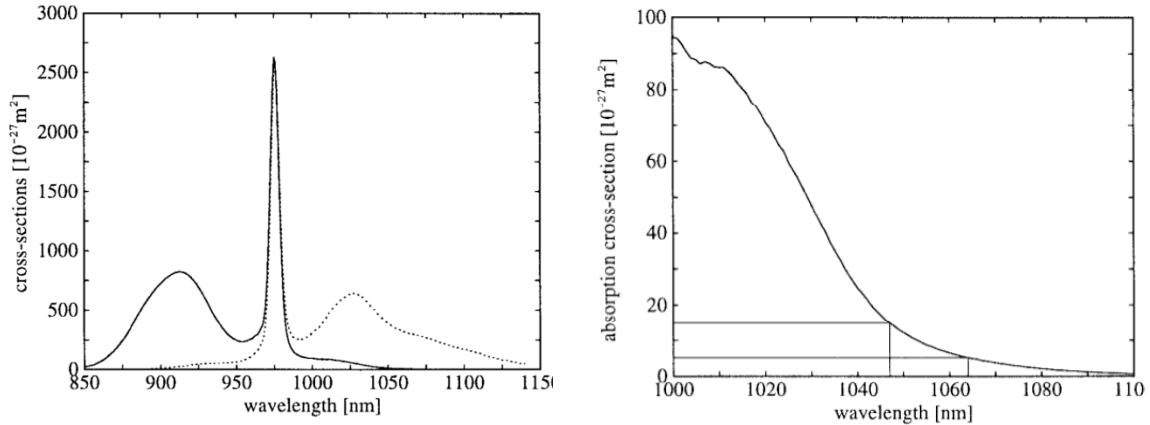


Figure 3-2: The absorption (solid) and emission (dotted) Spectrums of Yb Doped Fiber [16]

For the absorption there exists a broad peak centered at 915nm with a bandwidth of $\sim 65\text{nm}$ and a narrow peak at 975nm with a bandwidth of $\sim 15\text{nm}$. The narrow peak at 975nm can absorb about 3.3 times more than the shorter peak at 915nm. The emission gave almost a mirror image, with a large peak at 975nm with a bandwidth of $\sim 15\text{nm}$, and a broader smaller peak at 1030nm. Overlaying both the absorption and emission spectrum, it can be seen that there is a large overlap between the two. In Figure 3-2 (right) the absorption spectrum is showing that absorption exists for wavelengths as long as 1100nm. This is an important figure, as it is an indicator as to what wavelengths are susceptible to re-absorption in the Yb doped fiber and their relative re-emission as a longer wavelengths. This re-absorption is a key contributor in the spectral shaping of the ASE as the shorter wavelengths have a higher probability of being re-absorbed and emitted as longer wavelengths when there is more re-absorption present. The amount of re-absorption can be controlled in three ways, i) increasing the Yb doping concentration in the fiber and ii) increasing the length of the fiber effectively shifts the center wavelength of the ASE spectrum to longer wavelengths and iii) the driving pump power can be increased to saturate a larger portion of the doped fiber, which generally widens the

spectrum. Additionally, the output ASE spectrum can be shifted by varying the input-pumping wavelengths [17]. The affect of several different pumping wavelengths has previously been shown as well [16] and will not be covered extensively in this thesis. Both 915nm (SP-915-5-1015-7.5, Sheumann, MA) and 975nm (SP-975-5-1015-7.5, Sheumann, MA) pump laser diodes were used in this experimental setup. Both of these pump laser diodes provided a bandwidth ($<5\text{nm}$ FWHM) and a high maximum optical power output of 7.5W into a multi-mode fiber with a core diameter of $105\mu\text{m}$. The 915nm and 975nm wavelengths were chosen because of the discussed absorption efficiencies in Figure 3-2. The change in emission spectrum was experimented for 20m, 4m and 1m Yb doped fiber lengths.

3.1.2 Dual Core Fiber

There are a few ways to pump rare earth-metal doped cores for a desired emission spectrum. Core pumping is the least complex, where the pump-light directly propagates through the doped single-mode core. This is generally accepted for lower power pumping due to the smaller cross section of the single-mode core. Cladding pumping is where the pump light is propagating through the cladding and allows for a higher-powered pumping scheme due the larger cross-sectional area of the cladding. The novel dual-core Yb doped fiber (YBF, Prime Optical Fiber Corporation, Taiwan) was the chosen method of cladding pumping. The dual-core fiber consisted of two cores who are kept in optical contact. A multi-mode core with a diameter of $105\mu\text{m}$ is used for high-powered pumping, while the second core is Yb doped with a diameter of $5.2\mu\text{m}$. When the multi-mode core is pumped from a laser diode, the high optical power from the multi-mode core leaks into the cladding with a Yb-doped core to provide cladding. There exists

other methods for cladding pumping such as side pumping the cladding via V-groove, but the dual-core fiber produces more efficient results.

3.2 Laser Setup

The type of emission described in Section 3.1 is known as spontaneous emission. For the Yb to be used as a laser, stimulated emission must occur with population inversion in an optical cavity. In Figure 3-1, the upper state E_2 is a long-lived state and this allows for a large build up of electrons in E_2 until the number of electrons in the E_2 state exceeds the number of electrons in E_1 state, this is known as population inversion. During simulated emission, an incoming photon forces an electron to drop from E_2 to E_1 and this process creates a 2nd photon to be emitted with the exact same frequency as the incoming photon. Population inversion is important during stimulated emission, as it requires a higher probability that the incoming photon will stimulate an electron from E_2 to E_1 and emit a photon, as apposed to an incoming photon causing an electron to be excited from E_1 to E_2 . The setup proposed here is that the pump diode will pump electrons to E_3 , and fast transition down to E_2 will occur to have a large population built up at this level. Stimulated emission is then possible because of population inversion. To complete the laser, a cavity must be used to allow photon travel through the gain medium for stimulated emission. Several cavity designs are presented.

3.2.1 Ring Cavities

Given a cavity and with the presence of population inversion, a laser can be made. 4 different ring cavities were designed and tested to judge the dual core Yb-doped fiber's

ability as a gain medium and to determine an efficient lasing mechanism. The unidirectional propagation of the light in a ring cavity allowed for data measurements before and after the gain medium along a single path of light as apposed to a more difficult multi pass regime that a linear cavity would produce. For all 4 schematics, shown in Figure 3-3 and Figure 3-4, a single 976nm laser diode was used to optically pump 20m of Yb-doped dual core fiber with 1.2W of pump power. The remainder of the ring was made up of HI1060 fiber to allow for single-mode propagation in the 1060nm range. For Rings A-C, the coupler (FOBC-2-64-100-50-B-1-H-0, AFW, Australia), (Coupler 1) immediately following the gain medium is used as the output reading of the gain medium. PC1 (PLC-006-S25, PolaRITE, USA), the polarization controller is used to align the polarization state of the light for higher efficiency when reflecting onto the blazed grating (GR50-1210, Thorlabs, USA). The custom built circulator, C1 (1064 +/- 50nm, Aglitron, USA), had a double role as it was a means to insert the grating filter into the ring cavity and acted as an optical isolator to ensure unidirectional photon travel. The Input 1 (FOBC-1-64-100-10-B-1-H-0, AFW, Australia) coupler was used to calculate the low power going into the gain medium. The grating was adjusted from a well aligned vertically position to a misaligned position to incrementally decrease the efficiency of the filter to have a varied input into the gain medium. Once this measurement was done for several powers, it was repeated several times for different wavelengths to observe the gain seen over a broader spectrum. The several wavelengths that the grating was aligned to produce includes: 1057nm, 1065nm, 1075nm, 1085nm, 1095nm, 1105nm and 1115nm. Ring A was designed to test very low power input as the Input coupler added a 10dB loss (10%) while Ring B tested a higher input power with only a .46dB loss (90%). It is

expected that Ring B and Ring C will have very similar lasing characteristics, as the only difference is that Coupler 1 and Coupler 2 splitting ratios have been swapped. This allowed for a higher optical power to go through the filter and the 50/50 output will have a more spectrally filter output. Lastly, Ring D performed similar tests as Rings A-C with the optical circulator being replaced by a 50/50 coupler and optical isolators (ISOS-64-B-1-0, AFW, Australia). This setup was tested for its design trade-off. The custom built optical circulator had a relatively high insertion loss where the transmission from port 1 to port 2 suffered from a 0.75dB loss and port 2 to port 3 suffered from a 0.80 dB loss. Also, this component has a high cost compared to its replacement of a 50/50 coupler.

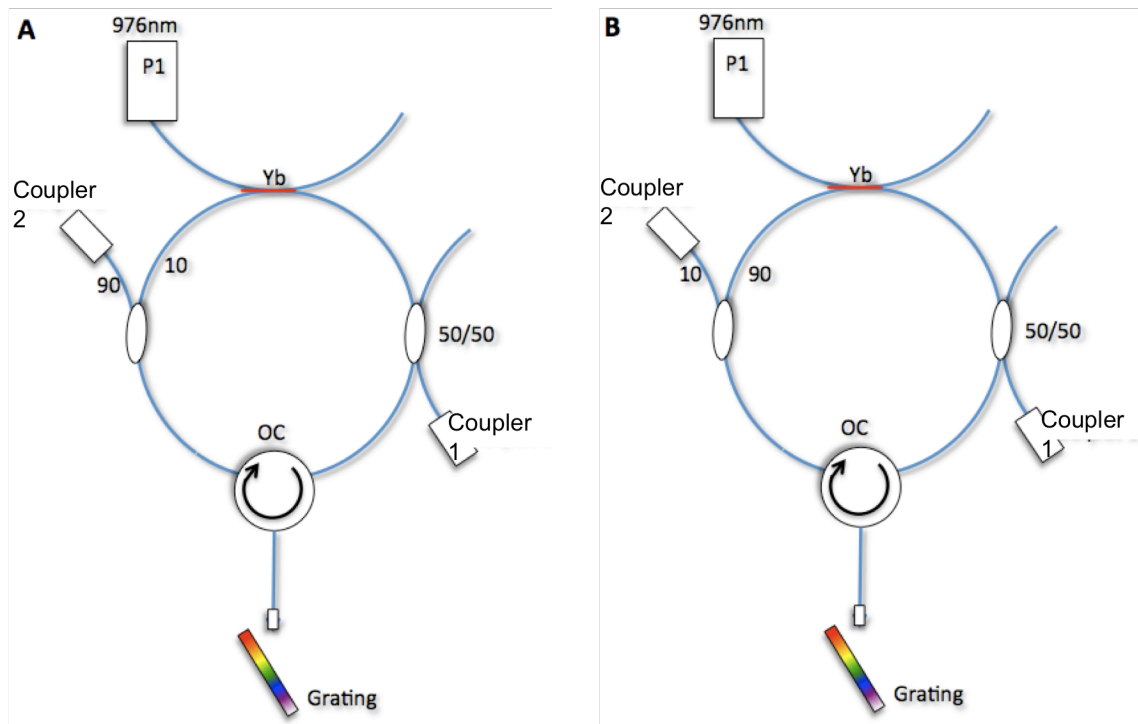


Figure 3-3: Ring cavities (A and B) setups to test the dual core Yb doped fiber as a gain medium

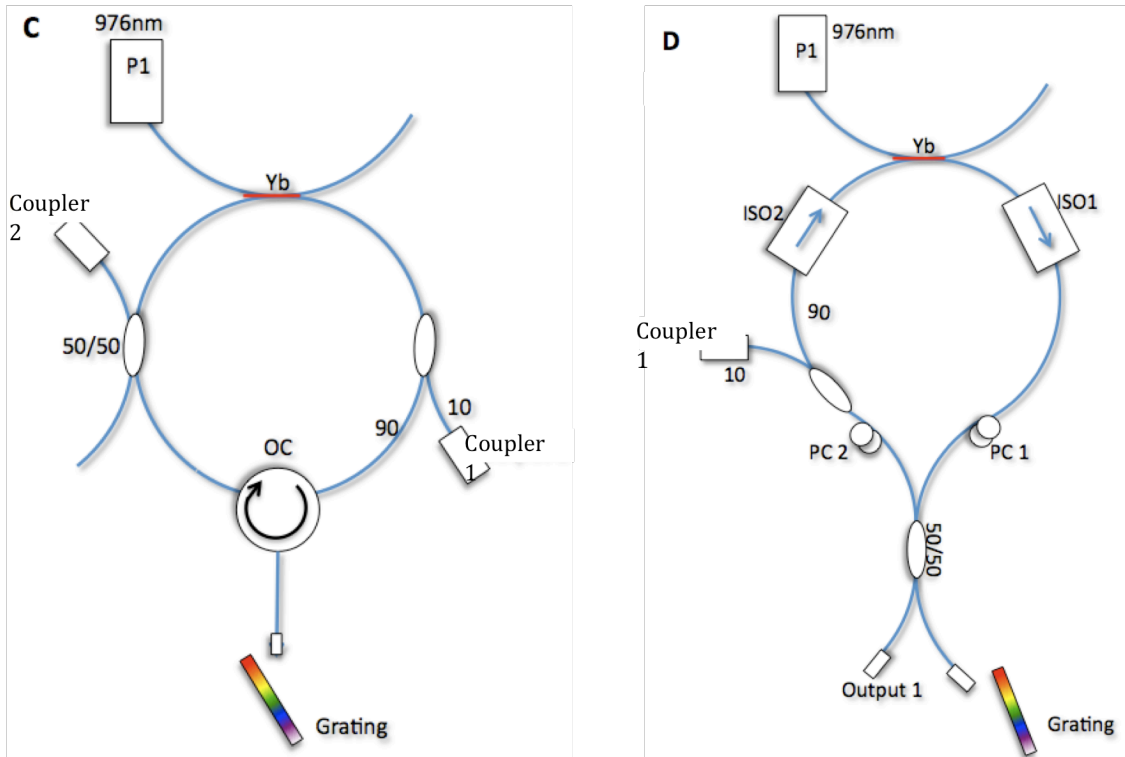


Figure 3-4: Ring cavities (C and D) setups to test the dual core Yb doped fiber as a gain medium

After the demonstrated use of Yb-doped fiber as a gain medium, Ring B was modified to be a swept source OCT laser. Two key components were added, a rotating polygon mirror and a swappable fiber spool (1.5 or 2.0km), to allow operation in both a short cavity and a long cavity.

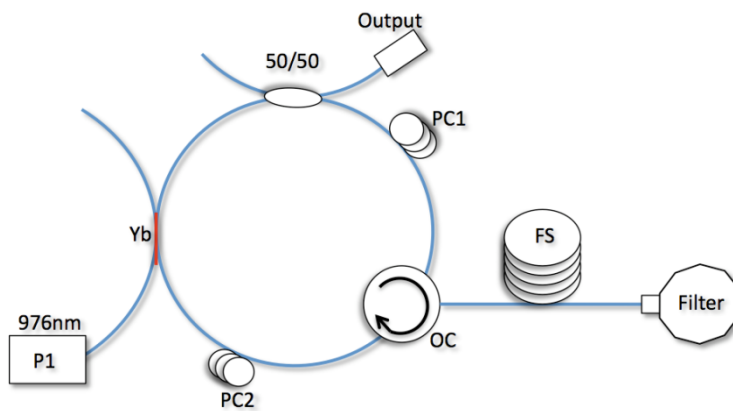


Figure 3-5: Wavelength sweeping ring cavity laser

The polygon filter selects a specific wavelength that is linearly ramped over time. The unfiltered (notch) light is used for stimulated emission on the Yb gain medium. The additions of a 1.5km or a 2km spool of HI1060 fiber onto port 2 of the optical circulator (OC) created effective lengths of 3km or 4km respectively due to the double pass in that fiber. The lengthening of the optical path in the ring cavity was necessary for Fourier Domain Mode Locked (FDML) operation.

3.2.1.1 Fourier Domain Mode Locking (FDML)

Fourier Domain Mode Locking (FDML) allows for a narrow bandwidth swept laser source to operate at a high scanning frequency without a loss to the signal to noise ratio. In a non-swept laser in a short cavity configuration (ex: Rings A through D), a single wavelength completes an infinite number of round trips within the cavity until the gain medium is saturated and the output power is at its maximum. In swept lasers in a short cavity, the amount of time allotted for photon round trip build up is not infinite, but is limited by the sweeping speed of the filter and the length of the cavity. If the filter sweep speed is increased, the build up time per wavelength is further reduced, which then becomes a limiting factor when trying to achieve faster OCT imaging. The length of the total cavity also governs the short cavity efficiency, as less fiber material in the cavity results in a shorter photon travel distance. A shorter distance corresponds to a faster photon round-trip time and allows for more photon build-up. In FDML, an optical delay is added by inserting a fiber spool into the cavity. The optical filter's repetition rate is tuned to have a period equal to the long cavity's photon round-trip time. This produces a quasi-station mode of operation. Light from an instantaneous position of the filter propagates through out the long cavity and when that specific wavelength of light re-

enters the filter, the filter will once again be tuned to that exact wavelength. Light from the previous round-trip is coupled back into the gain medium and stimulated emission of that specific wavelength is produced as well. An entire wavelength sweep from shortest to longest wavelength is stored within the entire span of the spool.

For FDML operation to occur, the following criterion must be met [18]:

$$f_{drive} = \frac{c}{l_{fiber}n} \quad \text{Eq. 3-1}$$

Where f_{drive} is the repetition rate of the optical filter, c is the speed of light in a vacuum, l_{fiber} is the total length of the cavity and n is the index of refraction of the fiber. The total length of the cavity used in this thesis was either 3km or 4km while the index of refraction of HI1060 fiber is 1.46. Using Eq.3-1, the repetition rate of the optical filter was calculated to be 51.4kHz and 68.5kHz for 3km or 4km lengths respectively.

3.2.1.2 Polygon Mirror Filter

In swept source OCT there are 2 popular sweeping filter configurations. The piezo-tunable filter can achieve high speed tuning with a sinusoidal bi-directional scan, where the wavelengths are swept from short to long and long to short [19]. Where as the polygon scanner is a saw-tooth uni-directional scan where the wavelengths are swept only from short to long. The unidirectional sweeping scheme has been shown to produce better OCT images [20]. The polygon configuration described in Figure 3-6 [17,21], had coupled the light into a collimator (HPUCO-23A-1300/1550-S-8AS-SP, OZ optics, Ottawa) to have a $1/e^2$ beam waist of 2mm to hit a 72-facet gold plated polygon mirror (SA34, Lincoln Laser, USA). The rotating polygon mirror provided a 10° sweep on a

high-groove density blazed grating (GR50-1210, Thorlabs, NJ). With the grating positioned at the Littrow angle, the 1st order would be reflect a specific defracted wavelength back to the polygon and back into the collimator. As the polygon rotated a different incident beam hit the grating causing a different defracted wavelength to be reflected. The Littrow angle was calculated using the grating equation [22]:

Eq. 3-2

Where d ($0.83\mu\text{m}$) was the period of the grating, θ_m is the diffraction angle, θ_i is the incidence angle normal to the grating, λ (1085nm) is the center wavelength and m is the order number. For a the first order ($m=1$) in Littman configuration, the incident angle is the same as the defracted beam, $\theta_m = -\theta_i$, which reduces the grating equation to:

$$2d \sin \theta_{m_i} = \lambda \quad \text{Eq. 3-3}$$

With a center wavelength of 1085nm , the Lithrow angle was found to be 40.8° from the normal of the grating. Given a 10° sweep from the spinning polygon, the achievable bandwidth is calculated as $\sim 219\text{nm}$ ($971\text{-}1190\text{nm}$). A total spectral width of 219nm was not seen, as the ASE of the gain medium did not cover that large spectral range. As a result, when the filter was tuned to a wavelength that was outside the ASE range, the output of the cavity was dead, as the Yb can not lase at these wavelengths.

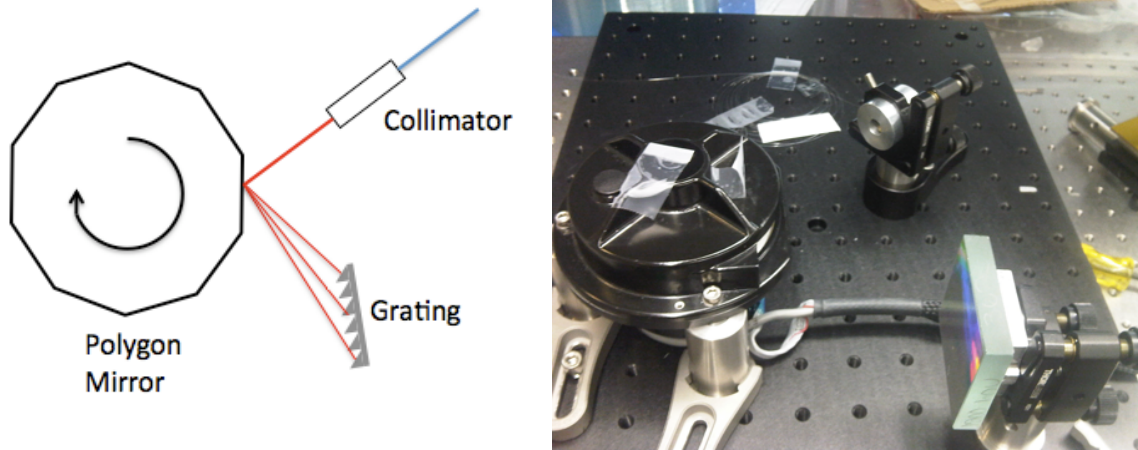


Figure 3-6: Polygon filter configuration, conceptual (left), actual (right)

3.2.2 Linear Cavity with Post Amplification

An alternative to the ring cavities for OCT swept source lasers is the linear cavity design with post amplification. The linear cavity will be known as the seed, and it provided a low powered sweeping source with an SOA gain medium, while the Yb was used for post amplification. No lasing occurs in the Yb doped fiber, but a single pass occurred for stimulated emission.

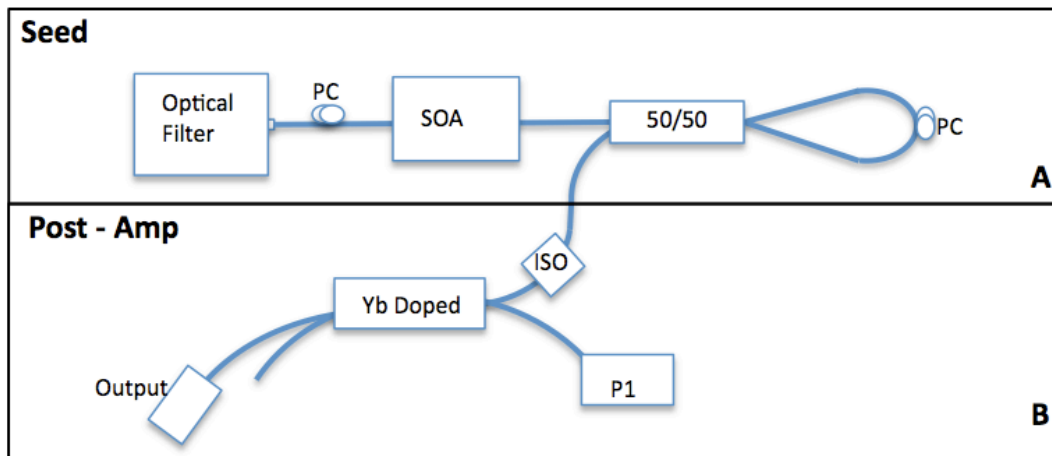


Figure 3-7: Linear cavity using Yb doped fiber as post amplifier

Figure 3-7 shows how the seed laser and the post-amp are used together. In the seed, the optical filter served as a “100%” reflective end of the laser while the two outputs on the opposite side of the 50/50 splitter was spliced together to create a the effect of a 100% reflective mirror. The coupler provided an output from the cavity while maintain 50% of the light for further lasing. An SOA gain medium (BOA-5391, Covega, USA) was placed in the middle of the cavity and a polarization controller (PC) was used to align the polarization states for higher lasing efficiency within the cavity. An isolator (ISO) was inserted between the seed stage (A) and the post-amp stage (B) to ensure that the high-powered gain medium does not burn any of the laser components. A similar pumping regime from P1 in the ring cavities in Figure 3-3 was used on the Yb. Various lengths of Yb doped fiber (20m, 4m, and 1m) were tested in this configuration.

3.2.3 Imaging Optics / Electronics

The imaging optics were configured in a standard OCT setup. An initial 90/10 splitter was used to tap 10% of the optical power for a clock signal. For the clock, the light was split into two separate paths via a 1x2 50/50 splitter and recombined by the 2x2 coupler for interference. The path difference in the two paths was ~2.5mm. A dual balanced photodetector (1817FC, Newport, USA) with a bandwidth of 80MHz converted the optical interference signal to an electronic signal. The remaining 90% of the coupler was sent to a Michelson interferometer. This was a fiber-based version of the interferometer presented in Figure 2-1, with an added circulator (C). In Figure 2-1 (interferometer), only 50% of the interference signal is sent to the detector while the other 50% is sent back to laser source. By inserting the optical circulator, the interference signal sent back to the light source was used with a dual balanced photodetector.

Although one interference signal from the interferometer would suffice, the signal to noise ratio can be increased by using the two signals. Both sample and reference arms collimated the beam and were reflected back with a matched path difference. The sample arm was reflected off of a computer controlled 2D scanning galvo mirror (6210H, Cambridge Tech., USA), through a focusing lens (AC254-030-C, Thorlabs, USA) and focused on to a sample. The scanning galvo mirror is used to position the focused beam at different sections of the sample; this provided a raster scanning mechanism. Figure 3-8 shows the imaging optics with the electronic interfaces. Blue lines are indicators of fiber optic mediums, red is an indicator of optics in free space, while black lines are indicators of electrical mediums.

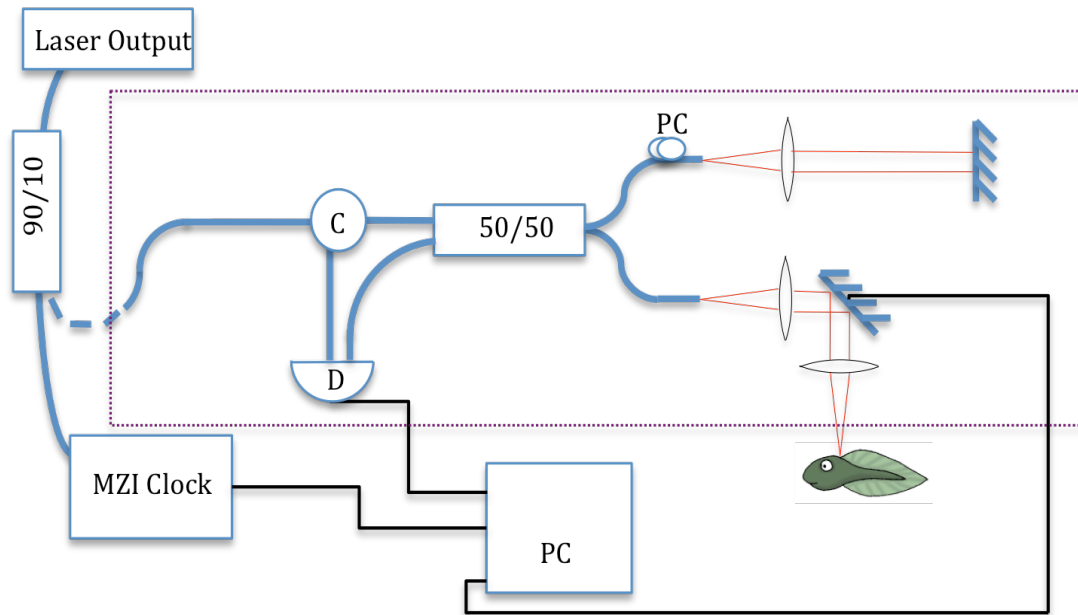


Figure 3-8: System diagram of imaging optics

The *in-vivo* sample that was imaged was a *Xenopus laevis* tadpole that has been matured for about 3 weeks. This sample was chosen as it is relatively optically transparent and its heart is located close to the surface of its body. The sample was anesthetized with

~0.01% Tricane until it became unresponsive to touch or vibrations. It was placed into a Petri dish with a sponge and shallow water with the ventral side up. The purple dashed box in Figure 3-8 represents the portion of the OCT setup where the high powered output is split into several output channels with multiple sample and reference arms.

4 Results

4.1 Amplified Spontaneous Emission Spectrums

Figure 4-1 shows the normalized ASE spectras in a dB scale of the dual-core Yb doped fiber for 3 different doped fiber lengths: 20m, 4m and 1m being pumped with a 976nm pump diode. Shortening the lengths of the doped fiber shifted the ASE peak wavelength down to shorter wavelengths while the edge-to-edge bandwidth was widened. Widening of the ASE spectrum is generally desired, as it allows fore a wider lasing spectrum, which in turn would increase the axial resolution as described by Eq.2-4. The highest tested output ASE power seen in the 1m of Yb was only ~7mW, while lengthening it to 4m and beyond allow for higher than 200mW. These results are summarized in Table 1.

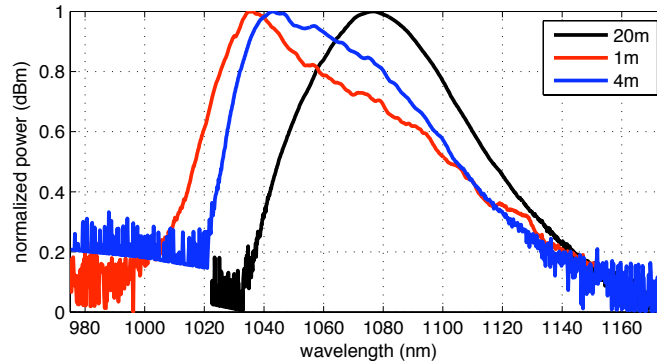


Figure 4-1: Amplified spontaneous emission of various Yb doped fiber lengths

	1m	4m	20m
Pump power	2.5W	2.5W	1W
Output power	7mW	>200mW	>200mW
Peak Wavelength	1036nm	1043nm	1076nm
Edge-to-edge bandwidth	119nm	102nm	95nm

Table 1: Summary of 3 Yb-doped fiber lengths

Another method for spectral shaping is by varying the pump wavelengths, two of which have been tested for in this study. Figure 4-2 shows an overlap of the two ASE spectrums. 976nm pumping provided an ASE with peak wavelength at 1075nm while a 915nm pump shifted the ASE peak wavelength to 1083nm. Overall, there was not a significant widening of the spectrum and it was not further investigated. Both of these spectrums were outputs of 20m of Yb doped fiber and it is projected that if the lengths of the Yb doped fiber are varied as well these ASE spectrums will be influenced in a similar fashion as in Figure 4-1.

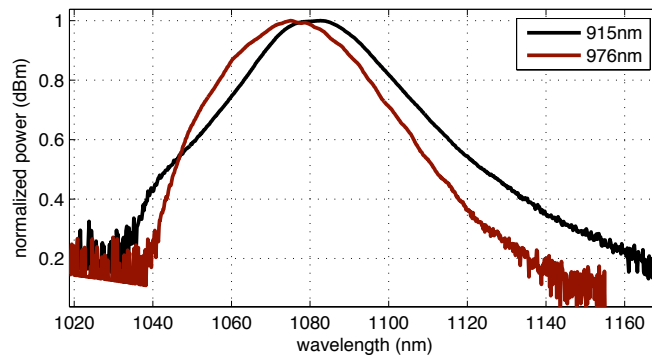


Figure 4-2: Amplified spontaneous emission of a 915nm and a 976nm pump

4.2 Ytterbium's Ability to Lase

The ytterbium provided lasing for several different wavelengths, which generally spanned the whole ASE spectrum. All of the cavities presented here are expected to have very similar linewidths as the exact same filter configuration and gain medium is used. The spectrums demonstrated in this section appear to have large linewidths ($>1\text{nm}$), but this is due to the resolution settings on the optical spectrum analyzer (86142A, Hewlett

Packard, USA) at the time of the measurement. An accurate depiction of the linewidth is shown in Figure 4-3 where the grating in the filter allowed the linewidth to have a 3dB bandwidth as narrow as 0.19nm.

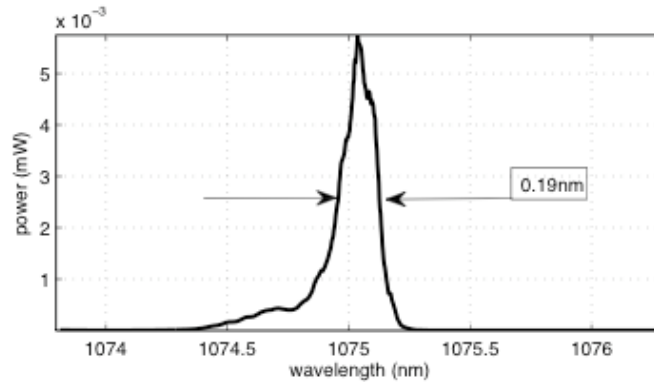


Figure 4-3: Linewidth of the filter

4.2.1 Ring A

Ring A tested the Yb-doped fiber's ability to lase with a low power input. Only two wavelengths were tested for, 1069nm and 1090nm and the outputs of Coupler 1 are shown in Figure 4-4. Both of these wavelengths provided expected lasing while the rest of the ASE spectrum was suppressed. Based in the results from Rings B through D, it is expected that if the filter's wavelength were to be changed to one that was towards the edge of the ASE spectrum (~1050nm or ~1120nm), there would not be as much suppression of the ASE. Figure 4-5 shows the gain of these 2 wavelengths as a function of input. As the power prior to the gain medium increased, it's gain decreased, showing that the gain medium is reaching a saturation state.

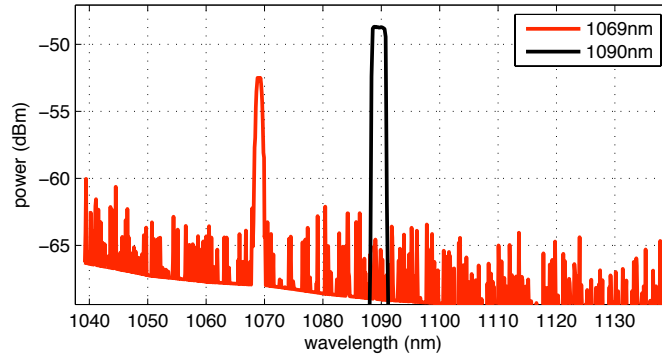


Figure 4-4: Lasing of different wavelengths in the Ring A configuration

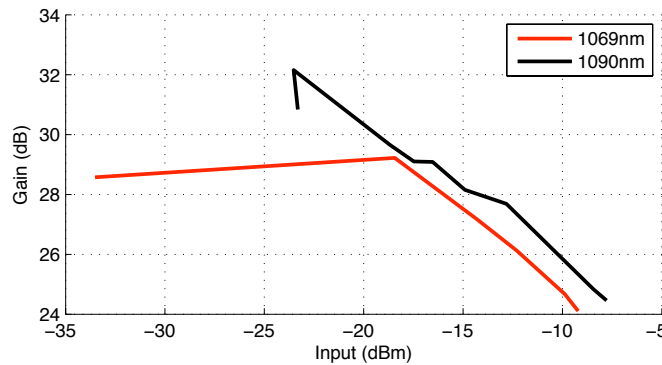


Figure 4-5: Gain of different wavelengths in the Ring A configuration

4.2.2 Ring B

Ring B's configuration was designed to test the Yb doped fiber's ability to lase with a higher power input compared to Ring A. A wide range of wavelengths was tested, which include 1057nm, 1065nm, 1075nm, 1085nm, 1095nm, 1105nm and 1115nm. Three of these wavelengths the output of Coupler 1 are shown lasing in Figure 4-6 with complete suppression of the ASE occurs during 1085nm lasing and only partial ASE suppression occurs during lasing at the ASE edges, 1057nm and 1115nm. Figure 4-7 shows the gain as a function of input. Wavelengths 1065nm to 1105nm exhibited saturation as the gain started to dramatically decrease as input slowly increased. For

1057nm and 1115nm saturation was not present and in comparison to the rest of the spectrum, a lower gain was seen.

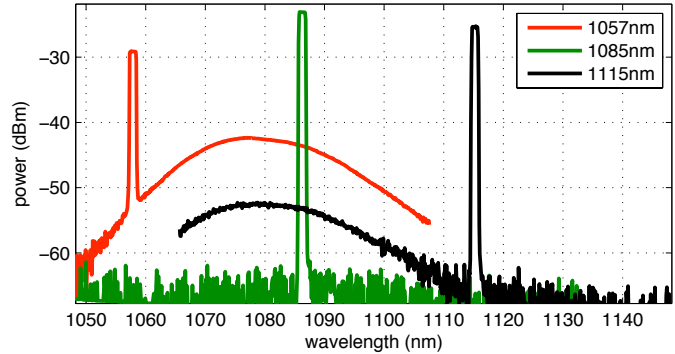


Figure 4-6: Lasing of different wavelengths in the Ring B configuration

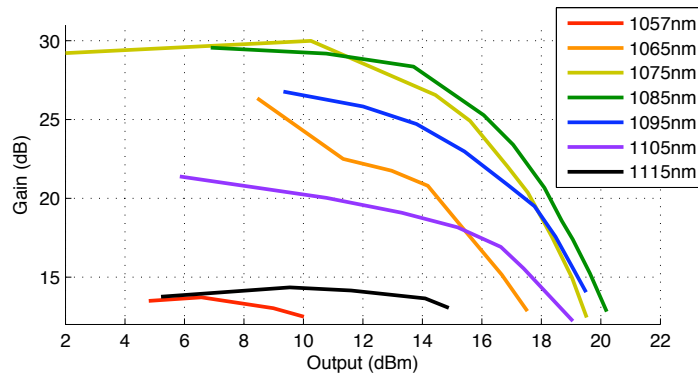


Figure 4-7: Gain of different wavelengths in the Ring B configuration

4.2.3 Ring C

As expected, Ring C's gain with several wavelengths (Figure 4-9) was very similar to that of Ring B's (Figure 4-7). The saturation of the gain medium was still seen, as the only difference was the order of components in the ring cavity. Figure 4-8 shows the output at Coupler 2 and the advantage of Ring C. A cleaner spectrum is seen as the unsuppressed ASE components of the spectrums have been optically filtered out due to the fact that the high-powered output is after the polygon mirror filter, as apposed to before the filter.

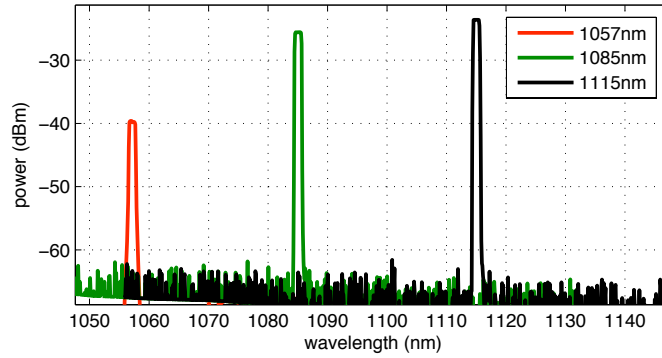


Figure 4-8: Lasing of different wavelengths in the Ring 3 configuration

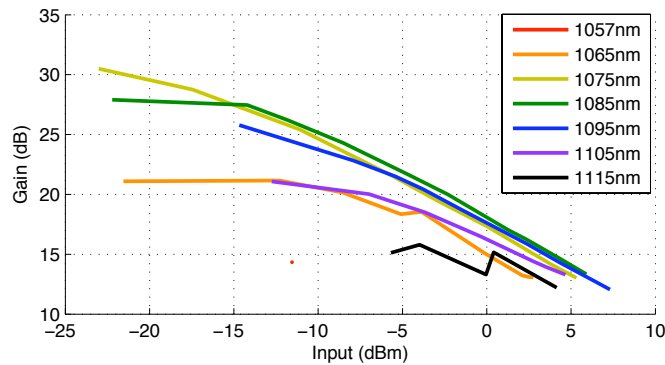


Figure 4-9: Gain of different wavelengths in the Ring 3 configuration

4.2.4 Ring D

Ring D was designed to test the lasing ability in a ring cavity that did not utilize a circulator to insert the optical filter. It was expected that the linewidths would have similar ASE suppression as in Ring B. It was uncertain of the efficiency of using a 50/50 splitter as a means to insert the filter as apposed to the circulator. Test results showed that the 50/50 splitter was not as efficient as the circulator, as there was a small reduction in output power. With a 50/50 splitter, the back reflected light from the polygon got split into two directions into the ring. One direction is amplified by the Yb doped fiber while an optical isolator attenuates any light propagating in the opposite direction.

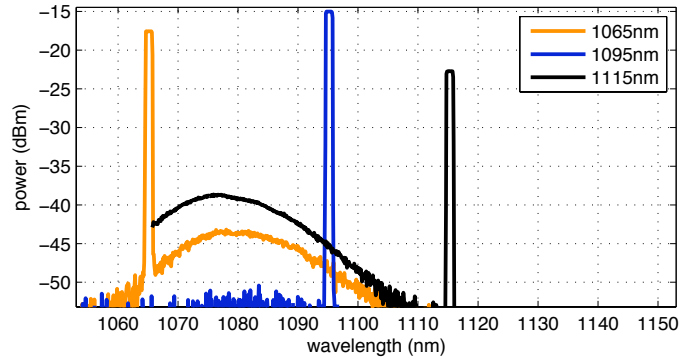


Figure 4-10: Lasing of different wavelengths in the Ring D configuration

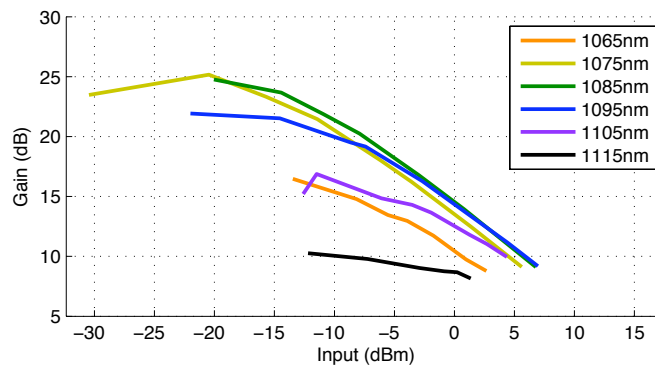


Figure 4-11: Lasing of different wavelengths in the Ring D configuration

4.3 Noise & Gain Figures, Polarization Extinction Ratio (PER)

Figure 4-12 demonstrates a narrow bandwidth output before Yb doped pumping and after Yb doped pumping in a single pass amplification scheme. There was a gain of 6.36dB, however, this is not the absolute maximum gain that can be achieved, and higher gain is possible if free space components are used with higher pumping regime. The burning threshold of the fiber optic component limited this gain. The polarization extinction ratio between the linearly polarized component and the horizontally polarized component 130.92 before a single pass amplifier and a ratio of 104.11 after the amplifier.

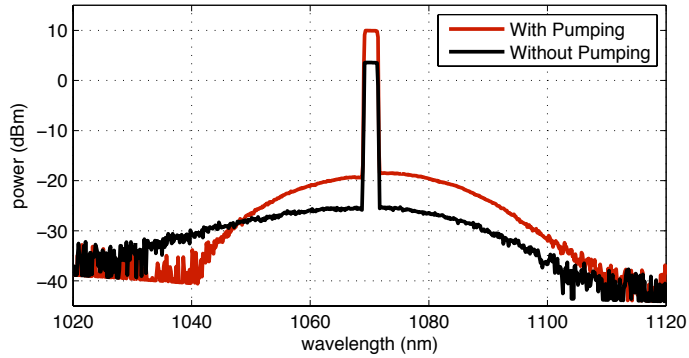


Figure 4-12: Gain and noise measurement data

4.4 Wavelength Sweeping Laser Source

Two regimes were designed and tested for the wavelength-sweeping source. A short cavity design was tested along with a long cavity with a delay fiber spool added to achieve FDML operation as described in Section 3.2.1.1. Both configurations generated very similar lasing bandwidths. The lasing bandwidth demonstrated in Figure 4-13 are the results from a 20m Yb doped fiber the Ring B configuration (Figure 3-3B) and was achieved by manually tuning the wavelength of the optical filter at a slow rate to allow for lasing at every possible wavelength. This measurement was done to set an indicator of the widest achievable bandwidth of the system. This measurement provided a known achievable standard when tuning the system for both short and long cavities.

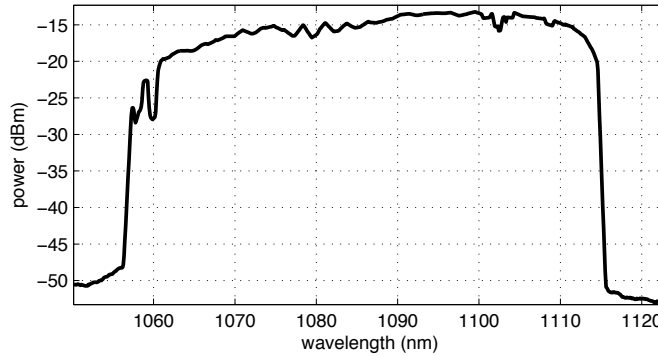


Figure 4-13: Lasing bandwidth seen from the Yb-doped fiber

The edge-to-edge lasing bandwidth ranged from 1057nm to 1121nm. A relatively flat top was achieved in the spectrum, which is generally desired in OCT light source design.

The noise component, such as the one seen at ~1060nm, is a measurement error as the filter was not manually set to those particular wavelengths for as sufficient amount of time for the OSA to completely observe it. It is expected that if the filter were tuned more slowly during the measurement the spectrum would create a smoother shape. A similar result was seen with 4m of Yb doped fiber where the lasing bandwidth extended lower than 1045nm. This result is expected based on the results seen in Figure 4-1 where the ASE spectrums for the different Yb doped lengths are shown. A spectrum with this type of bandwidth and power can generate good OCT images provided it maintains this shape when the light source is swept

4.4.1 Short Cavity

The ring cavity in Figure 3-5 was used without the fiber spool for the short cavity design, while utilizing a 4m segment of Yb doped fiber. The total length of the short cavity was ~5m and a relatively low sweep rate was tested. Typical short cavity polygon scanning systems with an SOA gain medium provides sufficient lasing with a 36kHz

sweep rate. Using the Yb doped fiber as a gain medium, required a slower sweeping rate as sufficient lasing was only seen when the sweep rate was less than 1kHz. Figure 4-14 shows the output spectrum as the source was sweeping slowly. Edge-to-edge lasing bandwidth spanned from 1049nm to 1131nm. During faster sweeps, drastic reductions in the bandwidth side lobes were seen. Although the bandwidth was larger enough it was deemed that the slow sweep rate of 1kHz was not fast enough for real-time imaging.

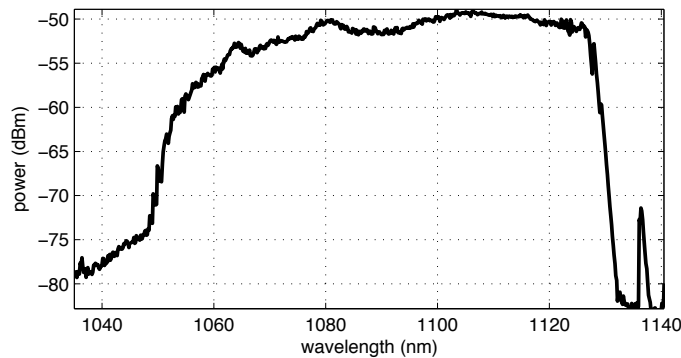


Figure 4-14: Output spectrum using 4m of Yb doped fiber in a short cavity

4.4.2 Long Cavity – FDML

The long cavity with a 1.5km spool that is described in Figure 3-5 was used for FDML operation. Because of the quasi-stationary state that the cavity exists in, as described in Section 3.2.1.1, the signal to noise ratio is much improved at high sweeping speeds. During FDML operation, the system was lasing fully for only a small section of the edge-to-edge bandwidth. When the sweep rate of the polygon was slightly increased, the lasing bandwidth was shifted to a lower frequency. Figure 4-15 demonstrates the output spectrum for three different sweeping frequencies; $f_1 = 67.176\text{kHz}$, $f_2 = 67.428\text{kHz}$, $f_3 = 67.680\text{kHz}$. f_1 and f_3 appear to be reciprocals of one another. When the two spectrums are overlaid on one another, the lasing bandwidth is from 1045nm to

1102nm, however separately half of the spectrum has been drastically reduced, but not completely. The 3dB bandwidths of either of the spectrums were not wide enough to obtain high resolution OCT imaging. Improvement to these spectrum shapes can be included in the future to implement this configuration for imaging.

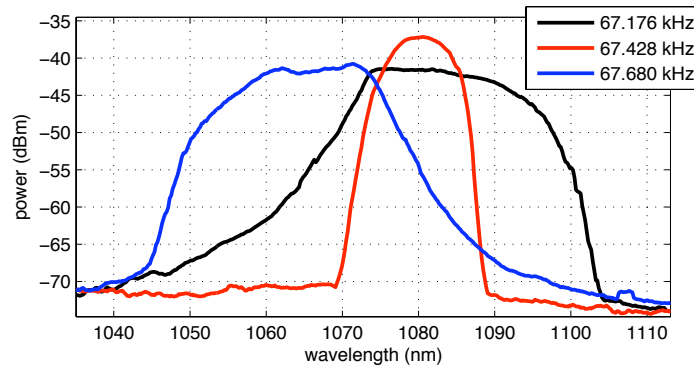


Figure 4-15: Output spectrum in FDML operation at 3 different sweeping frequencies

4.5 Yb doped fiber in Post Amplification Configuration

In a post amplification configuration, two different lengths of Yb-doped fibers were tested. 20m of doped fiber provided higher gain with re-absorption narrowing the spectrum. 4m of doped fiber provided a wider spectrum with less gain and lower re-absorption due to the reduced amount of Yb material.

4.5.1 20 Meters of Yb Doped Fiber

A 1060nm swept OCT laser source was constructed utilizing an SOA to create a seed laser. The output power was 5.4mW with an edge-to-edge bandwidth from 1038nm to 1098nm. The output spectrum of the seed laser is shown in Figure 4-16 in black. The seed laser had bi-directional wavelength sweeping (from 1038nm to 1098nm then 1098nm to 1038nm) at a rate of 8000 Hz. This light was passed through 20m of Yb doped fiber

where absorption occurred. With no external pumping to the Yb doped fiber, a significant portion of the bandwidth was lost due to absorption; this spectrum is shown in red and has a total output power of 0.5mW. The blue spectrum represents the spectrum when the Yb doped fiber is excited with the 976nm pump, which gave an output power in excess of 200mW. The output of the Yb doped fiber had both spectral amplification and broadening due to the external pumping. The bandwidth reduction caused by the absorption was an undesired artifact. To overcome the absorption issues, the seed laser could be pumped harder to reduced the overall effect of re-absorption, however a simpler solution would be to shorten the Yb doped fiber length.

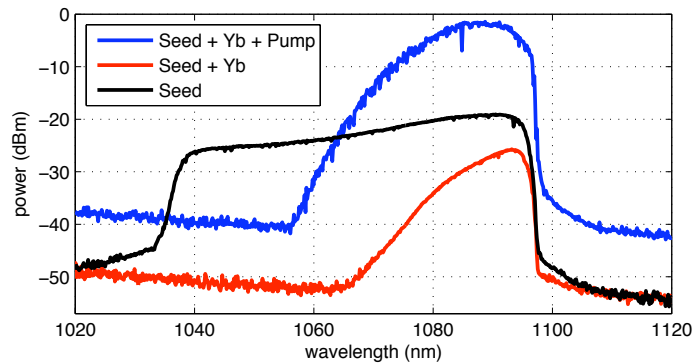


Figure 4-16: SS-OCT seed laser spectrum before and after 20 m of Yb doped fiber

4.5.2 4 Meters of Yb Doped Fiber

In comparison to Figure 4-16, it can be seen in Figure 4-17 that the shorter length of Yb doped fiber allowed for a 20nm larger bandwidth to pass through the gain medium without suffering from complete absorption. Given a very similar seed laser source, it can be seen that using 4m of Yb doped fiber over 20m of the same fiber provided a noticeably smaller spectral loss. This gain bandwidth is further expanded when the Yb doped fiber is pumped with a 976nm pump laser diode. A significant portion of the

entire edge-to-edge bandwidth was recovered by pumping the Yb with are large amount of power. Although the bandwidth of pre-amp and post-amp of the edge-to-edge bandwidth are very similar, spectral shaping occurred, causing the 3dB bandwidth to be drastically reduced in the post amp configuration. The seed laser demonstrated a relatively flat spectrum with a 3dB bandwidth of $\sim 57\text{nm}$, while in a post amp configuration, the spectrum had a slightly curved top, causing the 3dB bandwidth to be reduced to $\sim 35\text{nm}$ which subsequently affects the axial resolution governed by Eq. 2-4.

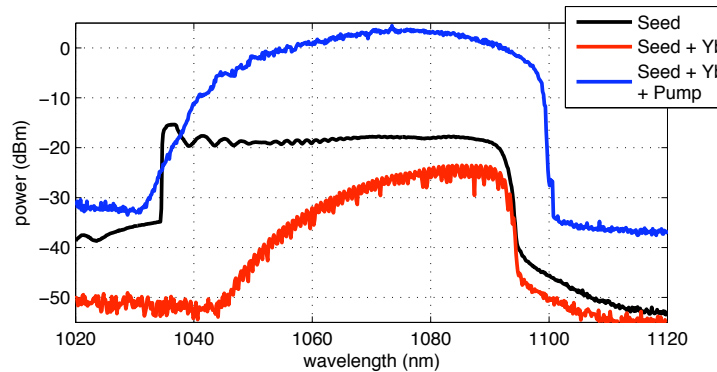


Figure 4-17: SS-OCT seed laser spectrum before and after 4m of Yb doped fiber

4.5.2.1 Point Spread Function

To further characterize this as a swept laser source for OCT imaging, the point spread function measurement was performed. A fiber optic Michelson interferometer is used with two gold plated mirrors located at matched distances in both the sample and reference arms. The reference mirror's length is varied for several distances and the back reflected interference signal is measured as a function of depth. A frequency oscilloscope took the measurement of the interference signal and it was saved for post processing.

This is an excellent indicator of the range in depth that the laser source can provide.

Simply put, this is an OCT image of a mirror at several depths. Figure 4-18 demonstrates the setup used.

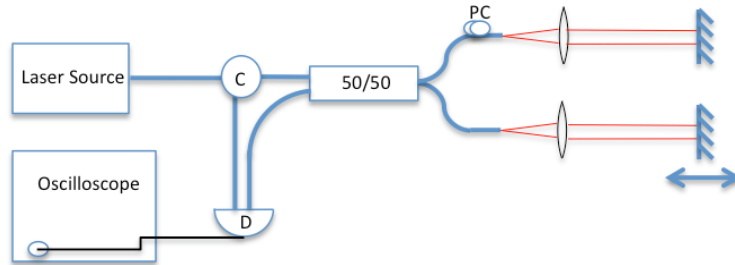


Figure 4-18: Interferometer setup for point spread function

By physically adjusting the position of the mirror, measurements were taken with a path difference of 0.0mm to 3.5mm with increments of 0.5mm while using the three configurations: 1) seed laser, 2) seed laser with 4m of Yb doped fiber with no pumping and 3) the seed laser with 4m of Yb doped fiber with high pumping (~4W).

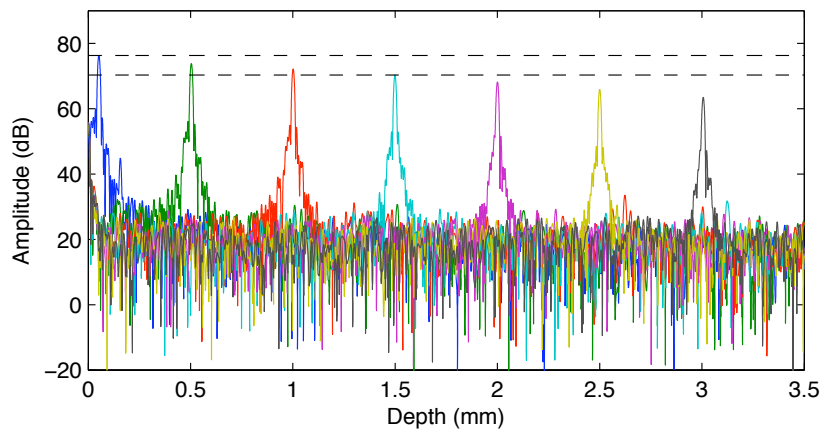


Figure 4-19: Point spread function measurement of the seed laser

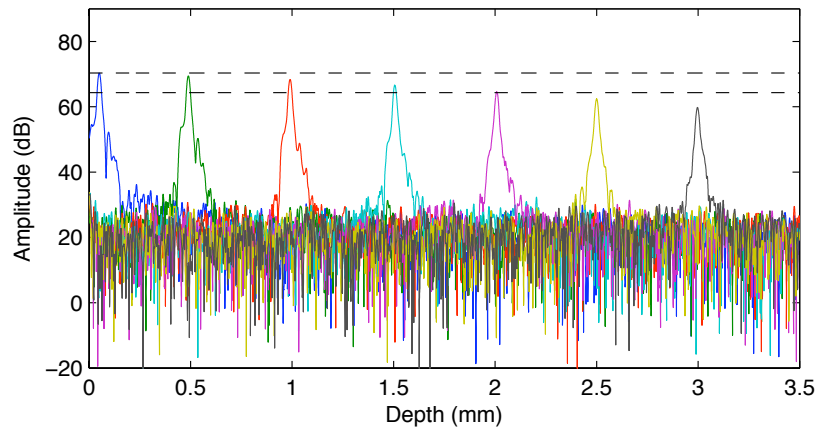


Figure 4-20: Point spread function measurement of the seed laser and Yb doped fiber without pumping

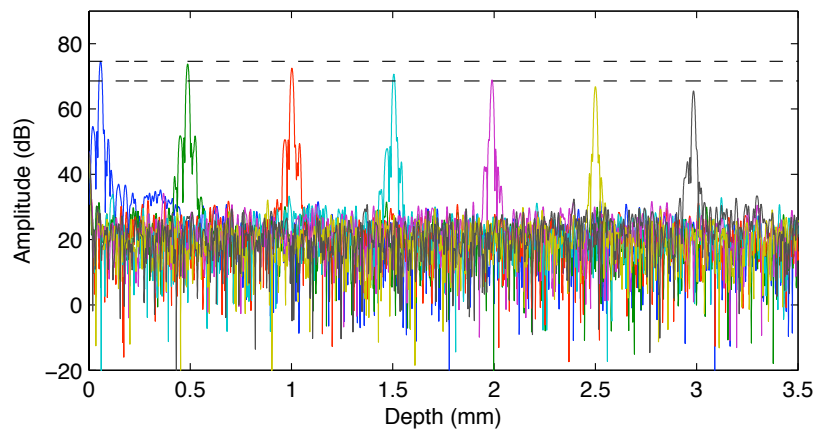


Figure 4-21: Point spread function measurement of the seed laser and Yb doped fiber with pumping

Figure 4-19, Figure 4-20, Figure 4-21 show the PSF measurements of the seed laser, seed laser & Yb doped fiber with no pumping and the seed laser & Yb with pumping respectively. The Fourier transform of the received interference signal is performed, as described by Eq. 2-6. The 6dB roll off from the 0.0mm position is a rough indicator of the physical range in which optimal imaging will occur, and this is a standard indicator set in the OCT industry. In the seed laser, this was measured to be at 1.5mm however, adding the Yb doped fiber lengthened the 6dB roll off of the point spread function measurement. The seed laser with the Yb doped fiber without pumping provided a 6dB

roll off of 2.05mm while pumping the Yb doped fiber provided a 6dB roll off of 2.25mm. For this measurement, the Yb doped fiber was pumped with approximately 4W from the 976nm pump. In general, narrowing the linewidth of the optical filter ($\Delta\lambda$) broadens this roll-off. The following table summarizes the dB drop-off as the reference and sample are varied in length:

Depth	Seed Laser (Drop off)	Seed + Yb + No Pump (Drop Off)	Seed + Yb + Pump (Drop Off)
0.0mm	0.00 dB	0.00 dB	0.00 dB
0.5mm	2.46 dB	0.90 dB	0.83 dB
1.0mm	4.14 dB	2.01 dB	2.12 dB
1.5mm	6.00 dB	3.74 dB	3.99 dB
2.0mm	8.12 dB	5.80 dB	5.75 dB
2.5mm	10.37 dB	7.96 dB	7.75 dB
3.0mm	12.84 dB	10.55 dB	9.11 dB

Table 2: Summary of the point spread function measurement

It must also be noted that the absolute amplitude values in the PSF measurements must not be considered as the signal power. The photo-detector has a threshold limit, where it will begin to saturate. For all the measurements, the output light from the amplifier was attenuated until the interference signal did not saturate the detector. Attenuating the light from the amplifier did not alter this measurement, as only the relative power loss from the 0.0mm position is considered. The reason for the saturation was because this test is very similar to imaging the surface of a mirror. In actual tissue OCT images, a significant smaller amount of light is back reflected from the sample, which causes the detector to not be saturated.

4.5.2.2 Clock Signals

The MZI clock described in Figure 3-8 was custom built, as a suitable clock mechanism is not commercially available for the 1060nm wavelength range. A clock is necessary in OCT as it is required for calibration for the interference signal. The construction of the MZI clock was done by tapping 10% of the total signal and splitting it equaling into two paths. The one path varied in length by 2.5mm and then the signals were recombined. The clock signal is generally desired to be a Gaussian shape, so that when Fourier transform operations are performed, no ringing artifacts are present.

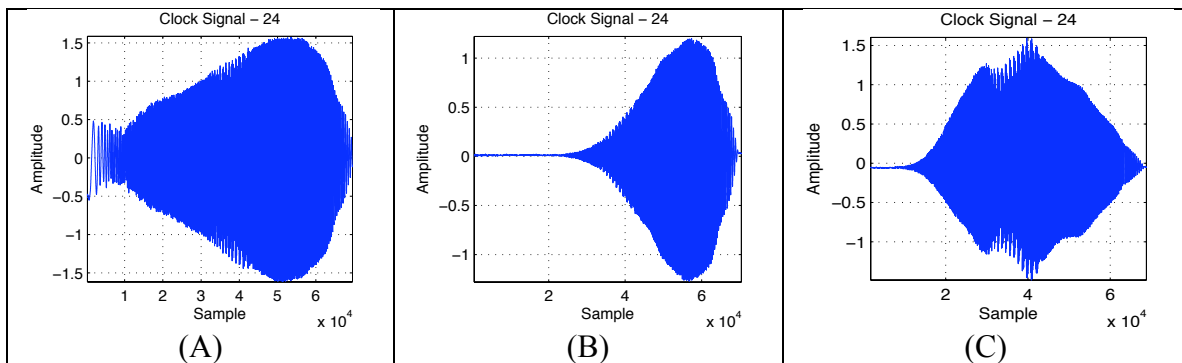


Figure 4-22: Clock signal of the laser source pre and post amp

Clock Signal A was taken directly from the seed laser source. Clock Signal B has the Yb-doped fiber added with no pumping and there was a significant lower amount of sample points, due to the fact that the output spectrum has also been reduced (Figure 4-17). Clock Signal C was taken when high pumping is occurring on the Yb doped fiber. Comparing Clock Signals A and C, A is larger in data sample size, meaning there are more data sample points from the interference signal. However, Signal C has more of a Gaussian shape to it, which is helpful when performing Fourier transforms

4.5.2.3 OCT Images

Multi-channelled images were obtained from the setup described in Figure 3-7 and Figure 3-8. A two channelled scanning head has not been devised so the two channels obtained were imaged separately and digitally stitched together during post processing. Figure 4-23 through Figure 4-25 show the cross sectional view of an *in vivo* image of the *Xenopus laevis* tadpole. The image sizes obtained had a resolution of 4096 x 512 and have been averaged by 4 in the transverse direction, which subsequently reduced noise and gave an image size of 1024 (transverse) x 512 (axial). The actual width of the image is 5mm (transverse) by 3mm (axial)



Figure 4-23: A 1-channel *in vivo* image (pre-amp) of a tadpole heart

Figure 4-23 demonstrates the seed laser as an OCT laser source. The 3-chamber heart is clearly visible along with several other structures of the sample. However, if this single laser source is split into two channels the light power to the sample is halved and the reduction in the signal to noise is clearly seen in Figure 4-24. The need for a high-powered

source for MOCT imaging is made very apparent here, as a lot of the deeper structure is not visible.

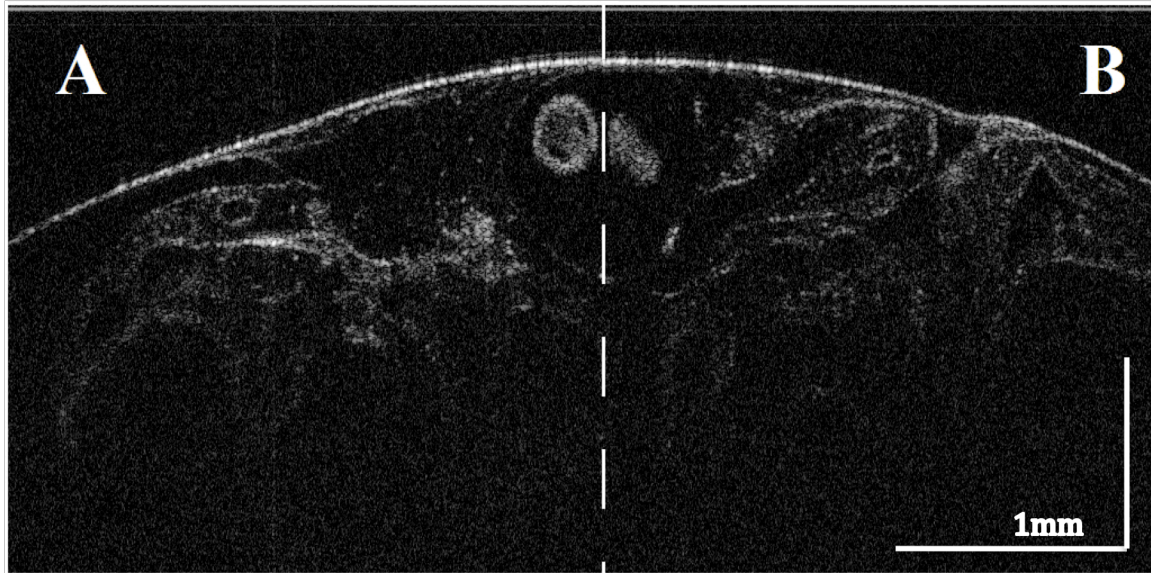


Figure 4-24: A 2-channel *in vivo* image (pre-amp) of a tadpole heart

After adding the Yb doped fiber in a post amplification configuration enough photons per channel were produced to image deeply. Figure 4-25 shows that amplification can then be further increased to penetrate further into the sample, as the bottom most layers in the sample are now visible again, and the loss seen in creating two channels has now been recovered. The power to each channel was approximately 20mW, which allowed for such a deep penetration. A minor problem that arose from the increase in power was that the photo-detector used to read the interference signal was suffering from saturation, causing odd streaks in the image, however this problem can be solved by adding even more channels.

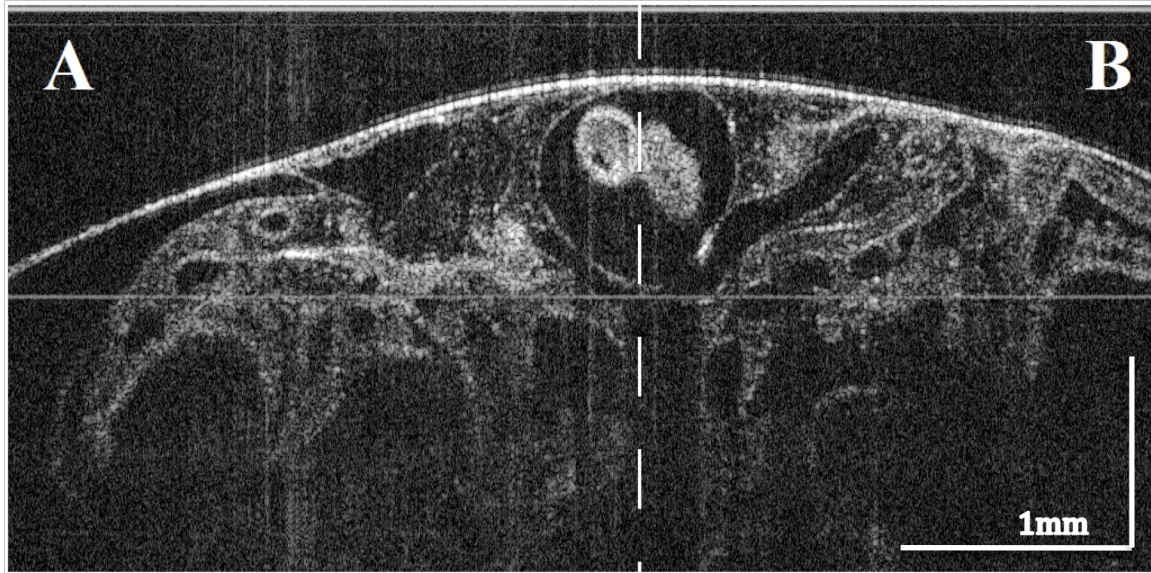


Figure 4-25: A 2-channel *in vivo* image (post-amp) of a tadpole heart

Full three-dimensional data sets were obtained of the *Xenopus Laevis* tadpole with a voxel resolution of 4096 x 512 x 512 corresponding to a 5mm x 5mm x 3mm volume.

5 Discussion

5.1 Ring Configurations

The four different ring configurations demonstrated the Yb doped fiber as a saturatable gain medium in a variety of setups. The wavelength range of these setups all were roughly centered at $\sim 1085\text{nm}$ which was reasonably close to the ideal 1060nm . For Ring B versus Ring C, the 50% output was placed before the circulator and optical filter as apposed to after the circulator respectively. Ring C's output had complete suppression of the ASE due to the filter's position in the cavity, not because of gain mediums lasing. However the drawback of Ring C is that the 50% output is slightly reduced by the efficiency of both the circulator ($\sim 1.5\text{dB}$ loss) and the filter ($\sim 1\text{dB}$ loss). Given the efficiency of the linewidth output, Ring B's configuration was chosen for both the short and long swept source laser experiments. Ring D was also a reasonable setup. If cost considerations are taken, a relatively expensive component such as the optical circulator can be replaced by a cheaper splitter. This swap will lower the overall lasing efficiency of the entire ring, but with such a large power being produced from the Yb doped fiber, the less efficient Ring D is a more suitable replacement.

5.2 Wavelength Sweeping Laser Source – Short

The length of the short cavity is related to the total output power. As the polygon filter spins, the instantaneous position of the filter will allow one specific wavelength to pass through. These photons propagate within the ring until it reaches the gain medium

again where it is amplified again and lasing begins. To increase the output power in this setup, the amount of roundtrips that can occur for a single wavelength need to be increased and this can be achieved in two ways; 1) the polygon filter can be slowed down to allow for a larger time gate or 2) the length of the ring can be shortened. A drastically reduced bandwidth ($<20\text{nm}$) was seen at standard sweep rates (36kHz) however when the sweep rate was slowed down to 1kHz the lasing bandwidth broadened to have a range from 1049nm to 1131nm. This would indicate that at 5m the total ring cavity length is too long or that 1060nm Yb gain medium generally requires more round trips to reach a saturation state in comparison to SOA based 1060nm laser systems. Given the required length of the Yb-doped fiber (4m), when a short cavity is necessary, this gain medium can only be used with slower acquisition times. Slower acquisition times are advantageous when a high sensitivity in Doppler imaging is needed, as a larger phase build-up between successive axial scans is possible, which may be a possible application of this slow scan rate.

5.3 Wavelength Sweeping Laser Source – Long (FDML)

In FDML operation, the spectrum shapes were reduced on either sides and they were also shifted by narrowly varying the sweep speed (Figure 4-15). This indicates that the gain medium does have the ability to lase at these wavelengths at the current sweep rate, and that the problem may come from chromatic dispersion in the HI1060 fiber spools.

5.3.1 Chromatic Dispersion in Fibers

When light propagates through a single mode fiber chromatic dispersion occurs. A perfectly monochromatic pulse width does not exist, as it will always have a defined bandwidth, $\Delta\lambda$. Because different wavelengths occur, the pulse width will have photons traveling at different speeds. With a range of speeds, a narrow pulse width is broadened inside a dispersive waveguide. The pulse widening is what hinders FDML operation in a highly dispersive medium, such as the HI1060 fiber.

5.3.2 Dispersion in FDML Operation

As described in the Section 5.3.1 chromatic dispersion leads to different wavelengths propagating at different speeds and this fact can be detrimental to FDML operation. The first condition for FDML operation stated in Eq. 3-1 simply solved that the sweep rate should equal the round-trip photon propagation time. In our case, with a 3km long cavity, the photon round-trip propagation time was 14.7 μ s (1/68kHz). However, given a highly dispersive medium (HI1060 fiber) the pulse width is broadened. This broadening can be quantified as:

$$\tau_{mismatch} = l_{fiber} d\Delta\lambda_{tuning_range} \quad \text{Eq. 5-1}$$

$\Delta\tau_{mismatch}$ (s) is the time delay between the shortest and longest wavelength after it has traveled through a given fiber length, l_{fiber} (m), where the fiber has a chromatic dispersion coefficient of d (ps/(nm x km)) and the light has a tuning range of Δ_{tuning_range} (nm). For successful FDML operation, the $\Delta\tau_{mismatch}$ must be smaller than the time duration τ_{gate} , where τ_{gate} is the time duration in which the bandpass filter transmits a single wavelength.

τ_{gate} can also be thought of as the dwell time that the system is lasing at a single wavelength, which is given as:

$$\tau_{gate} = \frac{\Delta\lambda}{f_{drive}\Delta\lambda_{tuning_range}} \quad \text{Eq. 5-2}$$

where $\Delta\lambda$ (nm) is the optical filter's bandwidth and f_{drive} is the filter frequency previously described in Eq. 2-1. Combining Eq. 2-1, Eq. 4-1 and Eq. 4-2 a criterion for a single successful photon round-trip propagation to occur in FDML operation can be described as:

$$\begin{aligned} \tau_{gate} &\geq \tau_{mismatch} \\ \frac{\Delta\lambda}{f_{drive}\Delta\lambda_{tuning_range}} &\geq l_{fiber}d\Delta\lambda_{tuning_range} \\ \Delta\lambda &\geq l_{fiber}d\Delta\lambda_{tuning_range}^2 f_{drive} \\ \Delta\lambda &\geq \frac{c\Delta\lambda_{tuning_range}^2 f_{drive}d}{n} \end{aligned} \quad \text{Eq. 5-3}$$

where c is the speed of light in a vacuum and n is the index of refraction of the fiber. The fiber being used in the cavity is comprised of HI1060 fiber. HI1060 is manufactured with a 5.3 μ m core for single mode propagation at 1060nm. However, at its single mode wavelength, there exists a large chromatic dispersion coefficient.

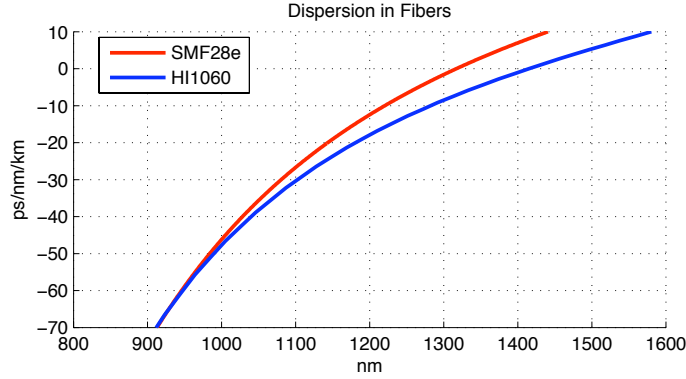


Figure 5-1: Dispersion curves for HI1060 and SMF-28 fibers

Figure 5-1 depicts dispersion curves for both HI1060 and SMF-28 fibers. In the SMF-28 fiber at ~1310nm, there exists 0 ps/nm/km dispersion which is why standard 1310nm OCT systems generally have no issues with dispersion. However in the HI1060 fiber at a 1060nm wavelength, there exists a -40 ps/nm/km dispersion coefficient. Given Eq. 5-3 with a $\Delta\lambda_{\text{tuning_range}}$ of approximately 90nm and an n of 1.46, the minimum linewidth is given as:

$$\Delta\lambda \geq \frac{3 \times 10^5 \text{ km/s} (90\text{nm})^2 40 \text{ ps/nm/km}}{1.46}$$

$$\Delta\lambda \geq 0.067$$

The filter bandwidth was tested to be 0.19nm, which satisfies the above condition. FDML operation was achieved (Figure 4-15) except for the odd spectral shaping that occurred at either the short end or long end of the spectrum, depending on the sweeping frequency. To further improve the FDML operation and reduce chromatic dispersion, a larger bandwidth filter ($\Delta\lambda$) could be used, however this would degrade the range in depth of the source. A second alternative would be to use dispersion compensation components such as dispersion shifted fiber (DSF) to shift the dispersion curve of HI1060 at 1060nm fiber closer to 0 ps/nm/km.

5.3.3 Accepted Work Involving Yb Doped Fiber for a Swept Source Gain Medium

The work demonstrating the Yb doped fiber as an OCT source was published as a manuscript in the SPIE Photonics West 2010 at the Fiber Lasers VII: Technology, Systems, and Applications conference with poster presentation also occurring at the Imaging Network Ontario (ImNO) Symposium 2010. The poster and manuscript are shown below:



Dual Core Ytterbium Doped Fiber Ring Laser in Fourier Domain Mode Locked Operation for Swept-Source Optical Coherence Tomography

Mark K. Harduar^a, Barry Vuong^b, Kyle H.Y. Cheng^b, Xijia Gu^a, Lawrence R. Chen^c, Beau A. Standish^a, Victor X.D. Yang^{a,d,e,f}

^aDept. of Electrical and Computer Engineering, Ryerson University, Toronto, Canada, ^bDept. of Electrical and Electronic Engineering, University of Hong Kong, Pokfulam, Hong Kong, ^cDept. of Electrical and Computer Engineering, McGill University, Montreal, Canada, ^dDept. Physics, Ryerson University, Toronto, Canada, ^eDivision of Neurosurgery, University of Toronto, Toronto, Canada ^fImaging Research, Sunnybrook Health Science Center



INTRODUCTION

- Optical coherence tomography (OCT) is a novel imaging modality that provides high-resolution images (~1-10 μm) suitable for real-time, *in vivo* imaging.
- A 1060nm wavelength light source is desirable because the light absorption and light scattering in water is at a minimum.
- Multi-channelled OCT requires a higher power output from the laser source due to parallel channels running simultaneously
- Ytterbium (Yb) doped fiber lasers can be used as a replacement for existing swept wavelength lasers for OCT due to its relative low cost of production and high power output.
- Fourier domain mode locking (FDML) of such a fiber laser may provide a high axial scan rate, which would make an optimal light source for current and future multi-channel OCT

AMPLIFIED SPONTANEOUS EMISSION RESPONSE

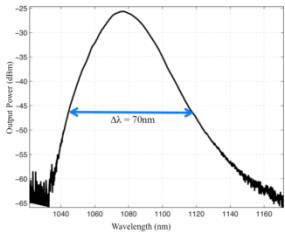


Figure 3: Amplified Spontaneous Emission (ASE) response of the Yb doped fiber with 976nm pump. Output power has been tested up to 237mW

SWEPT SOURCE LASER SPECTRUMS

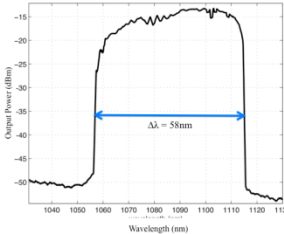


Figure 6: Full lasing bandwidth from a slowly tuned polygon filter. Tuning bandwidth spans 1057nm to 1115nm. The largest instantaneous output power tested was 60mW

EXPERIMENTAL SETUP

- A single 976nm pump laser drove a 20m segment of dual core gain medium
- High optical power leakage from the pump core creates population inversion in the doped core, which results in a broadband spectrum emitted from the dual core fiber into the ring cavity.
- A custom broadband 1064nm +/-50 circulator was utilized in the ring cavity to insert an optical polygon filter.
- The grating of this filter was setup in a Littrow configuration
- The circulator and filter components gave an ~10dB loss within the cavity.
- A 2km HI1060 fiber spool was used for an optical delay for FDML operation
- A better SNR was achieved because wavelength sweeping rate of 51.4kHz was achieved because of FDML.

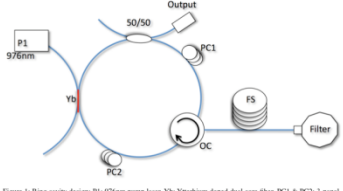


Figure 1: Ring cavity design: P1: 976nm pump laser, Yb: Ytterbium doped dual core fiber, PC1 & PC2: 3-port polarization controller, FS: 2km HI1060 fiber spool, Filter: Littrow polygon filter, OC: Optical Circulator

LASING OPERATION

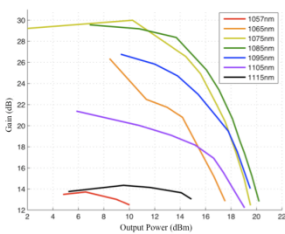


Figure 4: Gain of several different wavelengths. The plots of the center wavelengths show that this is a gain medium that can be saturated, which helps to improve spectral shaping.

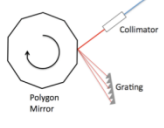


Figure 2: Telescope-less polygon scanner filter in Littrow configuration. Reflected light off the polygon mirror interrogated the blazed grating at an incident angle of 40°. The incident angle would vary by +/-5° depending on the instantaneous position of the polygon. Uni-directional sweeping was achieved.

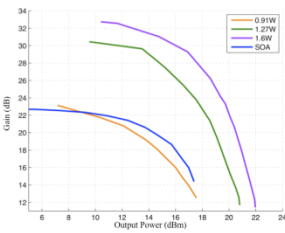


Figure 5: The gain is demonstrated for 3 different powers from the 976nm pump. This plot is also compared to a typical SOA lasing at 0° center wavelength

SUMMARY & CONCLUSIONS

- A novel dual core Yb doped fiber laser was designed for use in a FDML fiber ring cavity.
- High gain and wide tune-ability has been demonstrated for this gain medium.
- An ASE having a FWHM of 70nm and a lasing FWHM of 58nm are shown. If FDML operation is configured correctly, the sweeping bandwidth could be at least 58nm.
- The affects of increasing the 976nm pump power are that both the small signal and large signal gain of the Yb doped fiber laser are increased.
- Both ASE and lasing configurations were tested to have output powers of ~200mW with the potential to be in the wattage range.
- The immediate application of this new laser is to combine it with a multi-channel OCT system, where a single output power is split into several parallel channels for simultaneous imaging, while maintaining a sufficient SNR during high-speed 3D visualization of biological tissues.

REFERENCES: 1) Paschotta, R. et al. "Ytterbium-doped fibre amplifiers," *IEEE Journal of Quantum Electronics* 33(7), 1049-56 (1997). 2) R.Habee, et al. "Fourier domain mode locking at 1050nm for ultra-high-speed optical coherence tomography of the human retina at 236,000 axial scans per second" *Optics Letters* 32(14), 2049-2051 (2007). 3) Leung, M. et al. "High-power wavelength-swept laser in Littrow telescope-less polygon filter and dual-amplifier configuration for multi-channel optical coherence tomography," *Optics Letters* 34(18), 2814-2816 (2009).

ACKNOWLEDGEMENTS: Natural Sciences & Engineering Research Council of Canada, Cancer Care Ontario, Ryerson University

Dual Core Ytterbium Doped Fiber Ring Laser in Fourier Domain Mode Locked Operation for Swept-Source Optical Coherence Tomography

Mark K. Harduar^a, Adrian Mariampillai^b, Barry Vuong^a, Kyle H.Y. Cheng^c, Lawrence R. Chen^d, Xijia Gu^a, Beau A. Standish^a, Victor X.D. Yang^{a,e,f,g}

^a*Department of Electrical and Computer Engineering, Ryerson University, Toronto, Canada;*

^b*Department of Medical Biophysics, University of Toronto, Toronto, Canada;*

^c*Department of Electrical and Electronic Engineering, University of Hong Kong, Pokfulam, Hong Kong;*

^d*Department of Electrical and Computer Engineering, McGill University, Montreal, Canada;*

^e*Department of Physics, Ryerson University, Toronto, Canada;*

^f*Division of Neurosurgery, University of Toronto, Toronto, Canada;*

^g*Imaging Research, Sunnybrook Health Sciences Center, Toronto, Canada*

ABSTRACT

We demonstrate high efficiency and wide bandwidth gain in a Ytterbium doped fiber amplifier. The high-powered amplifier has potential applications for use with a swept-source fiber ring laser in multi-channel optical coherence tomography (OCT) system. The ring cavity design includes a 976nm pumped dual core Yb doped fiber as the gain medium, where a rotating polygon mirror is used as a wavelength-sweeping filter for this source. The amplified spontaneous emission (ASE) had a spectral bandwidth of 1037-1145nm at -60dBm, where a tunable lasing bandwidth of the ring cavity ranged from 1057-1115nm. The highest output power, for both the ASE and lasing spectrum, with this configuration was ~200mW, however it is possible to have a larger bandwidth and a larger output power. Higher power, in the wattage range is achievable if free space components are employed. Pumped with 976nm light at 1.27W, the use of this novel dual core Yb doped fiber as an amplifier has been successfully demonstrated, as it provided a small signal gain of 29.6 dB at 1085nm, where the gain medium was successfully saturated during operation. This is important for the spectral shaping requirements of OCT to improve image quality. The gain was demonstrated for several different wavelengths and for several pumping powers at a 1085nm wavelength. Fourier domain mode locked operation (FDML) was achieved with a bandwidth of 15nm and a sweep rate of 51.4kHz. This laser source offers a low-cost, high power alternative for biomedical imaging with multi-channel optical coherence tomography.

Keyword: Ytterbium doped fiber amplifier, optical coherence tomography, swept source, 1060nm, Fourier Domain Mode Lock

1. MOTIVATION:

OCT is a novel imaging modality that provides high-resolution images (~1-10 μm) suitable for real-time, *in vivo* imaging. It has also become a standard imaging technique for the retina and has demonstrated pre-clinical value in the detection of neo-plastic tissue and vascular lesions¹. Doppler OCT (DOCT) adds functional blood flow imaging and can be used to quantify hemodynamics down to the capillary level². Multi-channel OCT may improve the Doppler imaging performance³, however, there is an added requirement of several OCT channels, which requires a higher power output from the laser source prior to

splitting the light into the multiple channels. In addition, operating near the water absorption minimum (~1060 nm) will allow further imaging depth or penetration through saline, which will be a significant advancement in using OCT during surgical procedures. These imaging requirements necessitate the development of new sources. An example includes cladding pumped fiber lasers, such as Ytterbium (Yb) doped fiber lasers, as a replacement for existing swept wavelength lasers for OCT due to its low cost of production and high power output. Fourier domain mode locking (FDML) of such a fiber laser may provide a high axial scan rate, which could in turn produce an optimal light source for current and future multi-channel OCT and DOCT platforms.

2. INTRODUCTION / BACKGROUND

Recently, there has been a push for use of 1020-1120nm light sources for OCT retinal pathology imaging. This wavelength is desirable because the light absorption of water is at a minimum⁵. Using such a light source within this bandwidth range during biological imaging sessions can increase the light penetration in tissues such as vitreous humour or cerebral spinal fluid, with improved signal-to-noise ratio (SNR) and depth of imaging. Previously there has been development of swept source lasers within this wavelength range via conventional semi-conductor optical amplifiers (SOAs), but these output powers have been in the low milli-wattage range (<10mW). SOAs, as a gain medium, have been able to provide bandwidths of ~70nm. Like the SOA, the rare-earth element Yb can have its fluorescence spectrum tailored to be within the water absorption/scattering minimum. Ytterbium doped fiber amplifiers (YDFAs) consist of the rare-earth dopant fused within the glass silica of the optical fiber for amplification with high output power. An advantage that Yb has over other amplifiers, such as Erbium doped fiber amplifiers is that the Yb element only has one excited state manifold, which eliminates the possibility of unwanted fluorescence, which in turn improves the overall efficiency⁶. Paschotta *et al.* have demonstrated the absorption and emission spectra in Yb fiber from white light⁶. The absorption spectrum of Yb fiber is composed of a small broad peak at 915nm and a large narrow peak at 975nm. The fluorescence spectrum has been found to have a large narrow peak at 975nm and a smaller broader peak at 1030nm. Due to a significant overlap between the absorption and emission spectra, re-absorption can occur with the emission spectra. Re-absorption can be controlled in three ways i) changing the length of the fiber, ii) changing the doping concentration, effectively shifting the center wavelength of the ASE spectrum to longer wavelengths and iii) the driving pump power can be increased to saturate a larger portion of the doped fiber⁷. This last method shifts the ASE spectrum to shorter wavelengths and increases the overall optical power output. Additionally, different pump wavelengths can also vary the ASE spectrum. Fourier domain mode-locked (FDML) is an operational mode of a wavelength swept laser source, which allows for a higher sweeping speed while maintaining the SNR of slower scanning speeds. Effectively a quasi-stationary mode of operation is created. FDML allowed for photon build up within the filter line-width by matching the sweeping period with the round trip time within the cavity⁸. In this manuscript, a specifically designed ASE spectrum was used within a ring cavity to demonstrate the broadband gain around the water absorption minimum and the high efficiency of an YDFA for use as an FDML swept-source single and multi-channel OCT imaging platforms.

3. EXPERIMENTAL SETUP:

Several ring configurations were investigated. The optimal design is demonstrated in Figure 1. The entire system was assembled with HI1060 fiber, which allowed for high-power single mode operation at 1060nm but also added a loss of 1.5dB/km. A single 976nm pump laser (FWHM = 5nm) drove a 20m segment of dual core gain medium (YBF, Prime Optical Fiber Corporation, USA). The dual core medium was made up of a multimode pump core (118 μ m) side-fused to a single-mode Yb doped core (5.3 μ m). High optical power leakage from the pump core creates population inversion in the doped core, which results in a broadband spectrum emitted from the dual core fiber into the ring cavity. Given the high gain and the efficiency achievable with the Yb-doped fiber laser, a 3dB coupler was used to provide the high-power output while in the closed ring configuration. A custom broadband (1064nm +/-50, Aglitron, USA) circulator was utilized in the ring cavity to insert the polygon optical filter. The polygon filter acts as an

intra-cavity tunable wavelength filter to provide a sweeping wavelength output suitable for OCT imaging. The grating of this filter was setup in a Littrow configuration as described in Figure 1b⁹. The spinning mirror consisted of 72 facets (SA34, Lincoln Laser, USA), which gave an optical sweeping angle of $\sim 10^\circ$. Using a Littrow's angle of 40.8° and a 10° sweep angle aligned to a high-groove density blazed grating (1200 grooves/mm, Thorlabs, NJ, USA), the filter's achievable bandwidth was $\sim 219\text{nm}$ (971-1190nm). The spinning polygon mirror produced a unidirectional wavelength sweep, as apposed to the bi-directional fabry-perot filter. It IS previously shown that unidirectional wavelength sweeping can reduce noise as apposed to the bidirectional sweeping¹⁰. The circulator and filter components gave an $\sim 10\text{dB}$ loss within the cavity. Although the Yb doped fiber gain medium was not polarization dependant¹⁰, two polarization controllers were added to optimize the polarization states to improve the efficiency of the grating. A 2km spool is inserted between the optical circulator and the polygon filter to add an optical delay to assist in the FDML operation. The total length added by the spool is 4km as light propagates through it twice in one round trip.

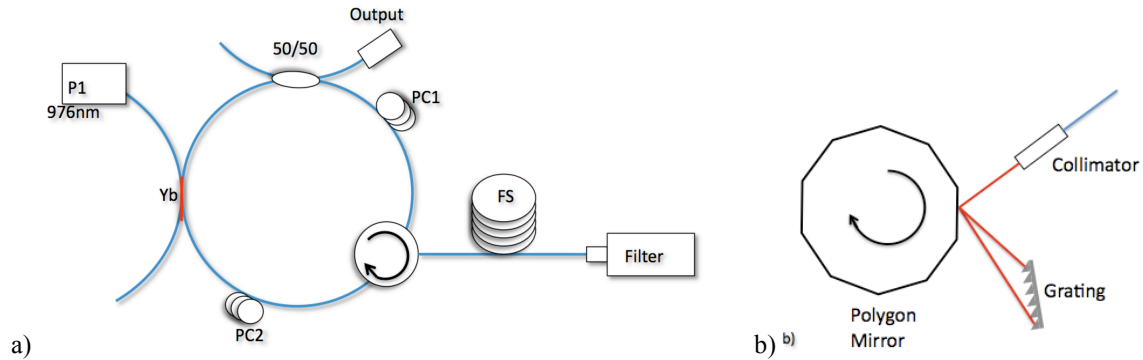


Figure 1. a) Dual core Yb doped fiber ring laser source for multichannel SS-OCT (P1: 976nm Pump Laser. Yb: Yb doped fiber (20m), PC: 3-panel polarization controller, C1: 1064 wide-band circulator). b) Polygon filter in a Littrow configuration.

For FDML operation, the optical filter's sweep rate was tuned to a period that is equal to a harmonic of the optical ring cavity's round trip time given by the following equation⁴:

$$f_{drive} = \frac{c}{l_{fiber}n}$$

Where f_{drive} is the scan frequency required for synchronization, c is the speed of light in a vacuum, l_{fiber} is the total length of the ring cavity and n is the index of refraction of the fiber core. Adding an effective length of 4 km of fiber (HI1060, Corning, USA) with an index of refraction of 1.46, the cavity's round-trip time is $19.3\mu\text{s}$, resulting in a 51.4 kHz sweep rate.

4. RESULTS:

4.1 Amplified Spontaneous Emission Response

Figure 2 shows the efficiency of the ASE optical spectrum of the Yb doped fiber created by the 976nm optical pump. It is hypothesized that there is a power loss from the pump to the Yb dual core fiber due to a core size mismatch, causing a poor fusion splice. For the given pumping range, a linear relationship was demonstrated. Based on slope in Figure 2, there is a 7.64dB loss by the dual core fiber. Figure 3a shows the output spectrum of the pump laser centered at $\sim 976\text{nm}$ with a 3dB bandwidth of 5nm. Figure 3b shows the ASE with our current Yb fiber length and pumping power. The peak is centered at 1076nm, with a FWHM of $\sim 25\text{nm}$ and an edge-to-edge bandwidth of 108nm (1037-1145nm). The highest tested ASE output power was 237.6mW. Based on the 976nm pump capabilities, the ASE has the ability to output in the wattage range. Power output in this range was not tested to avoid burning components.

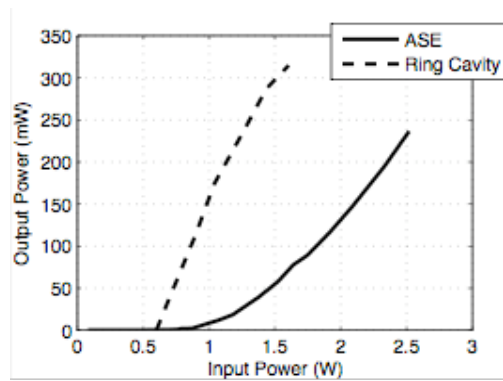


Figure 2: ASE and ring cavity laser output power based on 976nm input pump power.

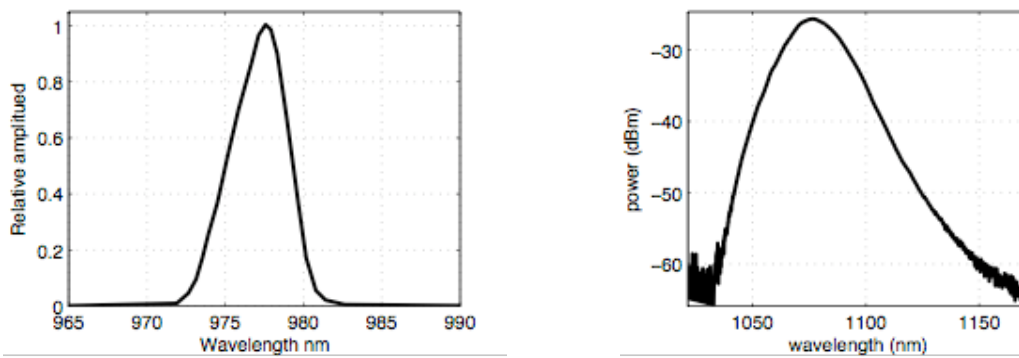


Figure 3: a) 976nm pump output spectrum. b) Dual core Yb amplified spontaneous emission output spectrum.

4.2 Yb Doped Dual Core Fiber as a Gain Medium

The Yb doped dual core fiber was tested for its use as a gain medium. Its gain was demonstrated for several wavelengths with varying input powers induced by a 976nm pump power of 1.27W. High gain was exhibited from the YDFA for a large spectral range, where gain saturation occurred around the center wavelength. It was observed that the side wavelengths of the lasing range did not reach the saturation regime. The lack of saturation on the sidebands can be viewed as an advantage, due to the ideal flat top spectral requirements of OCT laser sources. Figure 4a shows the gain with the filter tuned to 1057nm, 1085nm and 1115nm. The central wavelength has a small signal gain of 29.6dB, which is an improvement over the standard semi-conductor optical amplifiers (SOA's) small signal gain of ~23dB. The tested large signal gain also had a final output power greater than 20dBm. Having a larger pump power can increase the small and large signal gain; this trend is shown in Figure 3b. The SOA's (BOA 1017, Covega, NJ, USA) gain also shown for comparison.

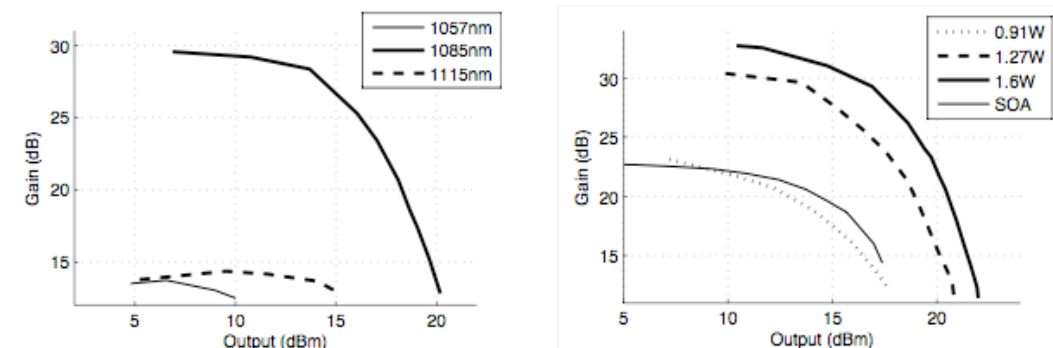


Figure 4: a) Gain of the Yb doped fiber at 1057nm, 1085nm and 1115nm wavelengths at a 1.27W pumping power. 1085nm demonstrates saturation. b) Gain in Yb doped fiber at 1085nm due to different pumping powers is compared to an SOA's gain curve.

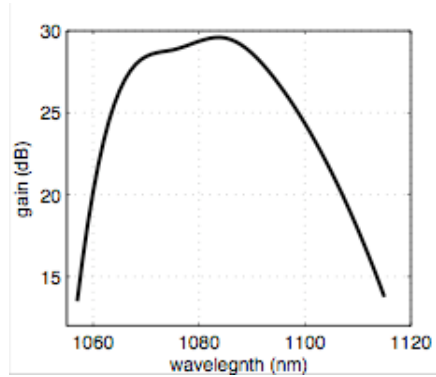


Figure 5: Small signal gain spectrum of Yb doped dual core fiber.

4.3 Sweeping Laser Source

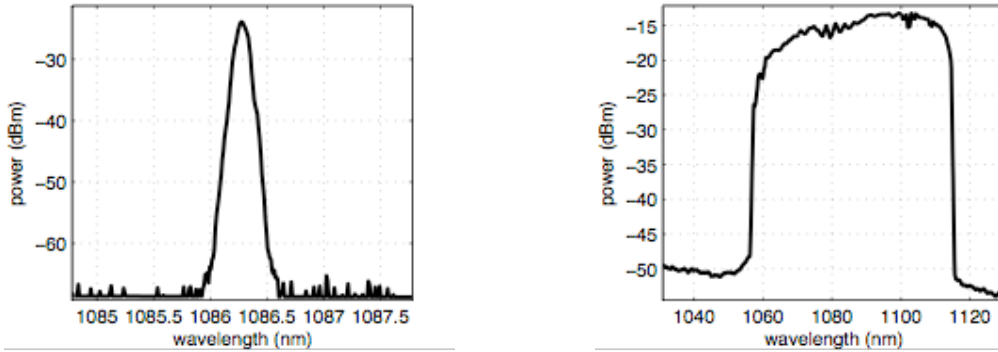


Figure 6: a) Instantaneous spectral line-width created by polygon filter. b) Laser output spectrum in a slow filtering short ring cavity

The ring cavity provided an instantaneous spectral bandwidth with a FWHM of $<0.15\text{nm}$ (Figure 6a). This instantaneous line width was able to sweep a range of 58nm (1057–1115nm). Figure 6b shows a peak hold mode of the instantaneous line-width manually swept at a slow rate (less than 1Hz). Figure 7 depicts the output spectrum when the filter speed was set to 51.4kHz in FDML operation. However, the spectral bandwidth was significantly reduced to a FWHM of 15nm with an optical power approximately 20mW .

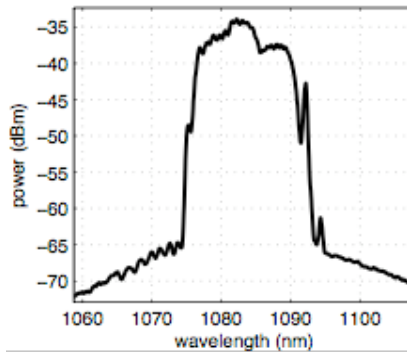


Figure 7: Laser output spectrum in FDML operation.

5. DISCUSSION:

The limiting factor in the system setup was that the fiber components have damage thresholds of 200-300 mW. A solution to this problem is to employ the use of free space optics in place of the optical circulator and splitters. Making these changes may allow for a dramatic increase of the output power into the wattage range. Despite the relatively large cavity loss, due to the custom made wide-band optical circulator (10dB), the ring cavity with the polygon filter proved to be a good method for lasing, as there was a large increase in output power (Figure 2). However, a sufficient pumping input of the 976nm pump was required prior to the center wavelengths of the gain spectrum reaching a saturation point. The sidebands of the gain spectrum still maintained non-saturation behaviour. This type of non-linear saturation contributed to the flat 'top hat' lasing spectrum in Figure 6b. Observing the results from Figure 4b, as the output power of the 976nm pump laser was increased, the ring cavity's lasing became more susceptible to saturation. Increasing the pump power can also further assist in the output spectrum flattening and widening. Given the bandwidth of 58nm, a ring cavity operating in an FDML setup should provide a similar spectral bandwidth, however the FDML operation dramatically reduced the bandwidth. It is speculated that this is related to the chromatic dispersion affect of the 4km of HI1060 fiber length and the 20m of Yb doped dual core fiber within the ring cavity. The chromatic dispersion caused by the fiber would cause different wavelengths to have a different cavity round trip times. The variation in round trip time across a wide spectrum can reduce the allowable lasing window in the FDML operation. If the correct dispersion compensation device is set up into the cavity such as a dispersion shifted fiber or a grating pair, the FDML spectral bandwidth should be widened to achieve similar results to the lasing output spectrum of Figure 5b.

Once the issue of the smaller bandwidth during FDML operation is resolved, the laser will further be characterized by a point-spread-function (PSF) to determine its ranging depth. Further more, OCT images will be obtained both on a single channel and a multi-channel system and any improvements over standard SOA systems will be compared and noted. Varying factors such as Yb pump wavelength and Yb fiber length will be explored to see its affect on ASE spectrum widening. Although the limitation of a ~200mW power output can be solved by using free space components, there is no immediate application for a swept source within the wattage range as the current output power is large enough for a 6 to 8 channel OCT imaging system.

5. CONCLUSION:

In summary, a novel dual core Yb doped fiber laser was designed for use in a FDML fiber ring cavity. High gain and wide tune-ability has been demonstrated for this gain medium. An ASE having a FWHM of 70nm and a lasing FWHM of 58nm are demonstrated. The affects of increasing the 976nm pump power are that both the small signal and large signal gain of the Yb doped fiber laser are increased as well. Both ASE and lasing configurations were tested to have output powers of ~200mW with the potential to be in the wattage range. The immediate application of this new laser is to combine it with a multi-channel OCT system, where a single output power is split into several parallel channels for simultaneous imaging, while maintaining a sufficient SNR during high-speed 3D visualization of biological tissues.

6. ACKNOWLEDGEMENT:

We would like to thank M.K. Leung and K.K.C. Lee for our discussions. This research was supported in part by Natural Science and Engineering Research Council of Canada (NSERC), Cancer Care Ontario and Ryerson University.

7. REFERENCES:

- [1] B. K. Courtney, N. R. Munce, K. J. Anderson, A. S. Thind, G. Leung, P. E. Radau, F. S. Foster, I. A. Vitkin, R. S. Schwartz, A. J. Dick, G. A. Wright, B.H. Strauss, Innovations in imaging for chronic total occlusions: a glimpse into the future of angiography's blind-spot. *European heart journal* Volume 29 Issue 5 (2008)
- [2] V.X.D. Yang, M.L. Gordong, B. Qi, J. Pekar, S. Lo, E. Seng-Yue, A. Mok, B.C. Wilson, A. Vitkin. "High speed wide velocity dynamic range Doppler optical coherence tomography (Part I): System design, signal processing, and performance" *Optics Express* 11, 794-809, 2003
- [3] Leung, M., Mariampillai, A., Standish, B., Lee, K., Munce, N., Vitkin, I., and Yang, V., "High-power wavelength-swept laser in Littman telescope-less polygon filter and dual-amplifier configuration for multi- channel optical coherence tomography," *Optics Letters* 34(18), 2814–2816 (2009).
- [4] Huber, R., Wojtkowski, M., and Fujimoto, J., "Fourier Domain Mode Locking (FDML): A new laser operating regime and applications for optical coherence tomography," *Optics Express* 14(8), 3225–3237 (2006).
- [5] B.Hermann, M.Esmaelpour, B.Povazay, B.Hofer, F. Bounaparte, N.Sheen, R.North, W.Drexler, "Wide field visualization of retinal and choroidal microstructure in vivo using frequency domain OCT at 1060 nm with up to 47000 lines/s ", *SPIE Vol. 7163, 71630A*, 2009.
- [6] Paschotta, R., Nilsson, J., Tropper, A., and Hanna, D., "Ytterbium-doped fibre amplifiers," *IEEE Journal of Quantum Electronics* 33(7), 1049–56 (1997).
- [7] D.C. Hanna, R.M. Percival, I.R. Perry, R.G. Smart, P.J. Suni and A.C. Tropper "An ytterbium-doped fibre laser: broadly tunable operation from 1010µm and three-level operation at 974nm", *Journal of Modern Optics*, 37(4), 517-525 (1990).
- [8] R. Huber, M. Wojtkowski, and J. G. Fujimoto, "Fourier Domain Mode Locking (FDML): A new laser operating regime and applications for optical coherence tomography," *Optics Express* 14, 3225-3237 (2006).
- [9] S.M.R. Motaghian Nezam " High-speed polygon-scanner-based wavelength-swept laser source in the telescope-less configurations with application in optical coherence tomography", *Optics Letters* 33(15), 1741-1743 (2008)
- [10] R.Huber, D.C. Adler, J.G. Fujimoto, "Buffered Fourier domain mode locking: unidirectional swept laser sources for optical coherence tomography imaging at 370,000 lines/s", *Optics Letters*, Vol.31 No.20 2975-2977 (2006)
- [11] R.Huber, D.C.Adler, V.J.Srinivasan, J.G.Fujimoto, "Fourier domain mode locking at 1050nm for ultra-high-speed optical coherence tomography of the human retina at 236,000 axial scans per second" *Optics Letters* 32(14), 2049- 2051 (2007)
- [12] M. Bashkansky, M.D. Duncan, L. Goldberg, J.P. Koplow, J.Reintjes, "Characteristics of a Yb-doped superfluorescent fiber source for use in optical coherence tomography", *Optics Express* Vol.3, No.8, 305-311, 1998.
- [13] S. H. Yun, G. J. Tearney, J. F. De Boer, N. Iftimia, and B. E. Bouma, "High-speed optical frequency-domain imaging," *Optics Express* 11, 2953-2963 (2003).
- [14] R. Huber, D. C. Adler, and J. G. Fujimoto, "Buffered Fourier domain mode locking: Unidirectional swept laser sources for optical coherence tomography imaging at 370,000 lines/s," *Optics Letters* 31, 2975-2977 (2006).
- [15] W. Y. Oh, S. H. Yun, G. J. Tearney, and B. E. Bouma, "115 kHz tuning repetition rate ultrahigh-speed wavelength-swept semiconductor laser," *Optics Letters* 30, 3159-3161 (2005).
- [16] Chen, L. and Gu, X., "Dual-wavelength Yb-doped fiber laser stabilized through four-wave mixing," *Optics Express* 15(8), 5083–5088 (2007).
- [17] M. Salhi, H. Leblond, F. Sanchez, "High power tunable all fiber double-clad Er:Yb:silicate fiber laser", *Optics Communications* 247 (2005) 181-185
- [18] M.Y. Jeon, J. Zhang, Q. Wang, Z. Chen, "High-speed and wide bandwidth Fourier domain mode-locked wavelength swept laser with multiple SOAs", *Optics Express*, 16(4) 2547-2554 (2008)
- [19] S.H. Yun, C. Boudoux, G.J. Tearney, B.E. Bouma, "High Speed wavelength-swept semiconductor laser with a polygon-scanner-based wavelength filter". *Optics Letters* 28(20) 1981-1983 (2003)

- [20] S.M.R. Motaghian Nezam, "High-speed polygon-scanner-based wavelength-swept laser source in the telescope-less configurations with applications in optical coherence tomography", *Optics Letters* 33(15) 1741-1743 (2008)
- [21] R. Herda, M. Rusu, S. Kivisto, O.G. Okhotnikov " Mode-locked ytterbium fiber laser with dispersion compensation by a fiber taper", *Ultrafast Phenomena XV, Proc. 15th International Conference. Pacific Grove, (2006)*
- [22] M. Rusu, R. Herda, S. Kivisto, O.G. Okhotnikov, "Fiber taper for dispersion management in a mode-locked ytterbium fiber laser", *Optics Letters*, 31(15) 2257-2259 (2006)

5.4 Post Amplification Configurations

5.4.1 Spectrums, Clock Signals, Point Spread Function

The Yb doped fiber successfully amplified the seed laser. Based on the Yb doped fiber output ASE spectrums the post amplification range can be predicted. A complete characterization of the Yb's gain spectrum based on fiber length was not formulated but based on the tested 1m, 4m and 20m lengths a rough estimation of the gain spectrum can be made.

An advantage that was seen by using the Yb doped fiber was the Gaussian shaping effect on the interference signals. This occurred because of the convenient overlap between the seed laser's output and the absorption spectrum of Yb. Although perfect Gaussian shaping did not occur, it did aid during noise artifacts in Fourier transform operations.

After calculating the point spread functions in Section 4.5.2.1, the 3dB widths of each peak signal can be analyzed for a direct measurement of the axial resolution. The seed laser gave an axial resolution of 9 μ m. The seed laser with the Yb doped fiber and no pumping gave an axial resolution of 15.8 μ m. The seed laser with the Yb doped fiber and pumping gave an axial resolution of 10.5 μ m. Adding the Yb reduced the axial resolution, which is expected due to the reduction in the spectral width, however the degradation from 9 μ m to 10.5 μ m is not a significant loss and is far out weighted by the advantage of the adding multiple imaging channels.

5.4.2 Image Analysis

The images for the multi-channelled post-amplification provided an increase in structural information. To help visualize this increase in structural information, the structural OCT images were enhanced in several ways through post-processing. The images were all normalized (1), meaning all the darkest pixel values were set as 0 and all the brightest pixels were set as 255, and all the values in between were all scaled accordingly. What this did is show the full dynamic range of the image. Secondly, a de-speckle algorithm was used where a 3x3 mask was applied to every pixel in the spatial domain (2). For every 3x3 mask location, the median was calculated and a new pixel value replaced the old one. The overall effect of this filter was to generally smooth out any sharp noises in the image. This process is effectively the same as a low pass filter in the frequency domain. The third filter applied was an edge detector to emphasize the structural information (3). The edge detector applied a derivative mask and edges were highlighted with white, while the background was suppressed to black. It was important to apply the de-speckle algorithm first so that background noise would not be mistaken for edges of the structural data. Lastly, a simple thresholding algorithm was applied to further differentiate background and structure (4). All pixel values that were less than 127 were automatically considered as background noise. Figure 5-2 shows the a flow chart of the algorithm sequence.

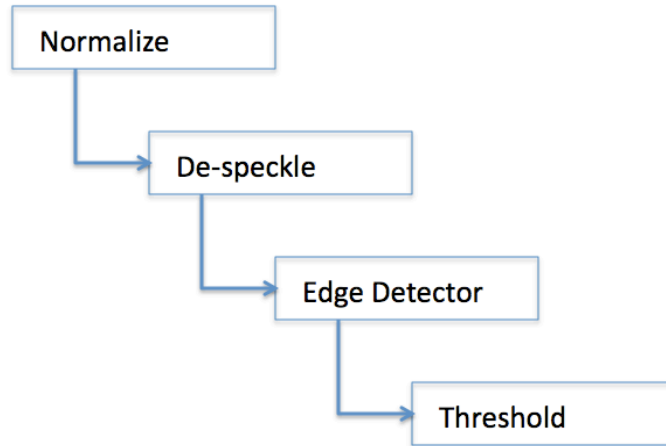


Figure 5-2: Simple structure detector algorithm

This type of image analysis is un-biased towards one side as both images were normalized and the exact same filters were applied in the same numerical fashion to images that were obtained from the exact same region of the same tissue sample.

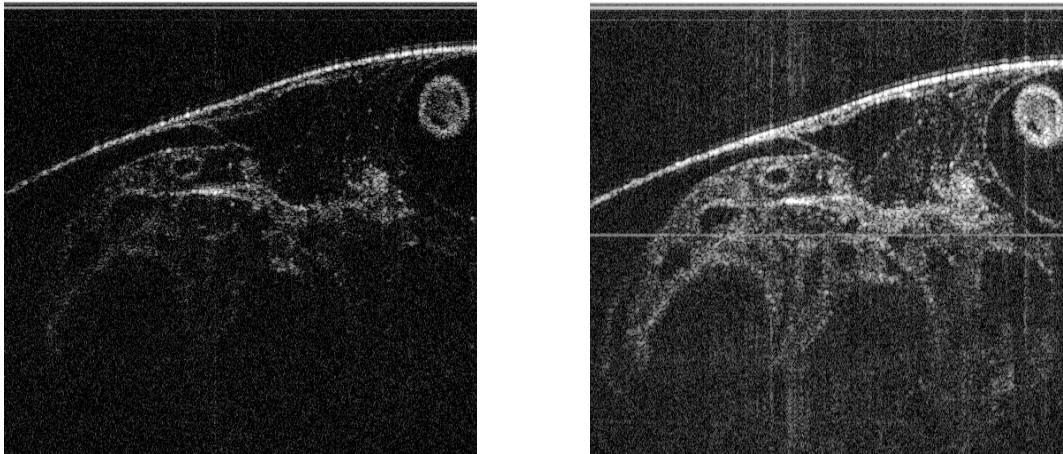


Figure 5-3: Structural image of channel A of MOCT image pre (left) and post (right) amplification

Post-amplification provided more structural information compared to pre-amplification and this is seen in Figure 5-3 and the difference is enhanced in Figure 5-4.

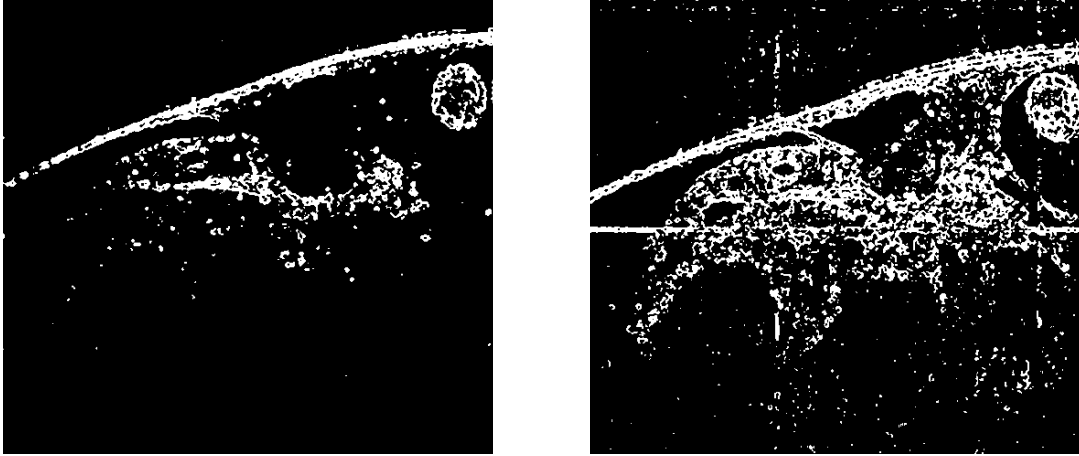


Figure 5-4: Structural detection of channel A of MOCT Imaging for pre (left) and post (right) amplification.

To further quantify these results, a total count of the white pixels can give a relative indication of how much structure is present in each image. From a total pixel count of 243942 per channel, the pre-amp had a white pixel count of 14273 (5.85%), while the post-amp had a white pixel count of 38354 (15.72%).

6 Conclusion

6.1 Summary

An OCT laser source, centered at 1060nm has been designed, developed, and produced. Dual core Yb doped fiber was utilized for high-powered amplification. The output ASE spectrums of the dual core Yb doped fiber have been characterized based on two different optical pumping wavelengths (915nm and 976nm) and three different fiber lengths (1m, 4m, and 20m). Both the 915nm and 976nm laser pump diodes provided similar output ASE spectrums with the 915nm's ASE spectrum being shifted to slightly longer wavelengths (+8nm). The two different pumping wavelengths did not provide a significant difference in the output spectrum. The shorter the Yb doped fiber length, the wider the output spectrum was, due to the lower probability of re-absorption into the fiber. If re-emission were to occur, the wavelengths would be emitted as successively longer wavelengths. However, with the shorter fiber, the output power was dramatically reduced as a smaller amount of gain medium existed. A 4m length of fiber was found to have a reasonable trade off, as the ASE spectrum spanned from 1024nm to 1124nm and output powers greater than 200mW was seen.

The Yb doped fiber was also placed into four different ring cavity configurations to test this gain medium's ability to lase under four different conditions. An optical filter in the form of a collimator and blazed grating allowed for a single wavelength lasing.

Lasing was successful for several wavelengths with greatest ASE suppression occurring for the center wavelengths (~1085nm). The gain of the Yb doped fiber due to different

input power was also measured to observe its ability to reach a saturable gain state, which is important for spectral shaping. Output powers of all the spectrums were all proportional to the power of the 976/915nm laser pump diode. The highest operating lasing wavelength was $\sim 200\text{mW}$, but it is projected that the output can be within the wattage range. Higher output power was not tested, as operational threshold of the components used were approximately 250mW .

This well characterized gain medium was also tested for its ability to work as a swept source laser. A sweeping filter was constructed with a 72-faceted spinning polygon mirror, grating and collimator and was inserted into the ring. The swept source laser was tested for two operations modes: a short cavity and a long (FDML) cavity. In a short cavity configuration, sufficient lasing occurred only during a slow sweeping rate of less than 1kHz . Although the observed output-sweeping spectrum was wide and powerful enough for good OCT imaging, the sweep rate was not fast enough. The slower sweep rate was a resultant of the relatively large portion of Yb doped fiber inserted into the short cavity. Each sweep required a longer time to lase because the photon trip length was also long. In a long cavity operation the cavity length was made to be 3km long and the sweep rate of the filter was tuned to the photon round-trip travel time in the cavity.

This allows for a high-speed sweeping rate without a loss to signal power. FDML operation was achieved, however the output spectrum had been reduced in width and odd spectral shaping and lower efficiency occurred due to the lower chromatic dispersion in the 3km of HI1060 optical fiber.

A third mode of operation was in a seed and post amplification configuration. The Yb doped fiber was taken out of the short cavity and replaced with an SOA. This

cavity configuration provided a low powered output but was able to optically sweep at an 8kHz rate. This output of the seed was coupled into the Yb doped fiber and acted as a single pass amplifier. The overall edge-to-edge spectral range was slightly narrowed by 10nm, but due to spectral shaping, the 3dB bandwidth was reduced from 60nm to 35nm. The output power was amplified from 10mW to more than 200mW, which is sufficient enough for multi-channel OCT.

Aside from the power benefits of using the post amplification configuration, this setup was tested for any degradation that the Yb doped fiber could have added to the swept source laser. Point spread function (PSF) measurements were performed to determine the axial resolution and range in depth. The axial resolution was degraded as expected: the measured 3dB width of the PSF signal was changed from 9.3 μ m to 10.5 μ m for the seed laser and seed laser plus amplifier configurations respectively. The range in depth was slightly improved as the 6dB roll off increased from 1.5mm to 2.25mm. An advantage that the amplifier had was the Gaussian shaping affect on the interference signal at several depths. With Gaussian shaping applied, cleaner Fourier transform operations can be applied resulting in an image with less artifacts.

Multi-channelled imaging was performed on a beating *Xenopus laevis* tadpole heart to demonstrate *in vivo* image. Two channels were used to show a single laser source can be split into several channels and provide consistent imaging. Through image analysis, it was numerically shown that the post-amplification configuration had improved the structural data in a MOCT system.

6.2 Future Work

With a seed laser providing sufficient imaging with 10mW and a tested output power of greater than 200mW, this setup has enough power for at least 10 channels with double the power. A full implementation of a 10-channel system simultaneously imaging would require 10 sample and reference arms and a well-designed raster scanning mechanism. Custom software would be designed to acquire 10 channels of data and process them all in parallel. Similar work has been done with 6 channels in the 1310nm range [9].

Although FDML operation was achieved in this thesis, there was significant degradation in the output bandwidth due to the chromatic dispersion in HI1060 fiber at 1060nm. Dispersion compensation devices can be employed to improve its operation. In such a high dispersive material ($d = -40$ ps/km/nm) and a large bandwidth of 80nm the time difference between the shortest wavelength and longest wavelength can be given by:

$$\tau_{diff} = |d| l \Delta\lambda$$

$$\tau_{diff} = 40(ps/km/nm) \times 3(km) \times 80(nm)$$

$$\tau_{diff} = 9.6ns$$

Where d is the chromatic dispersion coefficient, l is the length of fiber and $\Delta\lambda$ is the bandwidth. The physical difference in air between the shortest and longest wavelength can be given by:

$$l_{diff} = \frac{\tau_{diff} c}{n}$$

$$l_{diff} = \frac{9.6ns \times 3 \times 10^8 m/s}{\sim 1}$$

$$l_{diff} = 2.88m$$

With a path difference of 2.88m between the shortest and longest wavelength, larger free

space compensation will be needed, but an all fiber solution would be simpler. An alternative fiber can completely replace a portion of the HI1060, with a positive dispersion coefficient providing an effective dispersion coefficient 0 ps/km/nm. A reasonable insertion loss would not be a major issue, as the gain medium could be pumped harder for a higher output power.

Another fiber based dispersion compensation method would be to insert a chirped fiber Bragg grating. When broadband light pass through a fiber Bragg grating (FBG) one specific wavelength with a narrower bandwidth is filtered and reflected back to the light source. Inducing a periodic variation in the index of refraction in the fiber core can create the FBG. The period is chosen based on the reflected wavelength. In a chirped FBG, the wavelength specific reflectors are placed at different lengths in the fiber. When used with an optical circulator, the distance traveled by different wavelengths can be compensated. If a total distance of 2.88m exists between the longest and shortest wavelength, a chirped FBG should have a total length of 1.44m (2.88/2) in length, with the wavelength dependant FBG reflectors placed incrementally throughout the length of the fiber. Within the high dispersive medium, the longer wavelengths travelled at a faster speed than the shorter wavelengths, so the shortest wavelength FBG should be placed at a distance of 0m in the chirped FBG while the longest wavelength is placed at the end of the chirped FBG (1.44m). This configuration theoretically compensates for dispersion issues.

With OCT laser sources, for axial resolution improvements, larger spectral bandwidths are desired (Eq. 2-4). A second rare earth metal with a slightly varied emission spectrum can be utilized. Neodymium (Nd) has two absorption peaks at 808nm

and 869nm, while there exists 4 emission peaks, 946nm 1064nm 1123nm and 1319nm. The two emission peaks at 1064nm and 1123nm are suitable as they both fall within a desired output spectrum. Nd can be introduced into the current system by using co-doping, where the doped medium contains both Nd and Yb, which would be a simpler implementation. The other alternative is to combine two separate lasers along with various filters, where the Yb light will be multiplexed with the Nd light. The latter method provides more control as the variables (length and pump power) of each element can be controlled independently. Overall, an improved method for spectral shaping is possible.

Figure 6-1 is a proposed ring cavity that uses a dual Yb and Nd pumping scheme for a wider spectral output. The Yb and Nd are implemented independently, as apposed to a co-doped fiber so the pumping schemes can be controlled independently. A chirped fiber Bragg grating is added for dispersion compensation during FDML operation. A long period grating is added to the output for spectral shaping, allowing for a wider 3dB bandwidth.

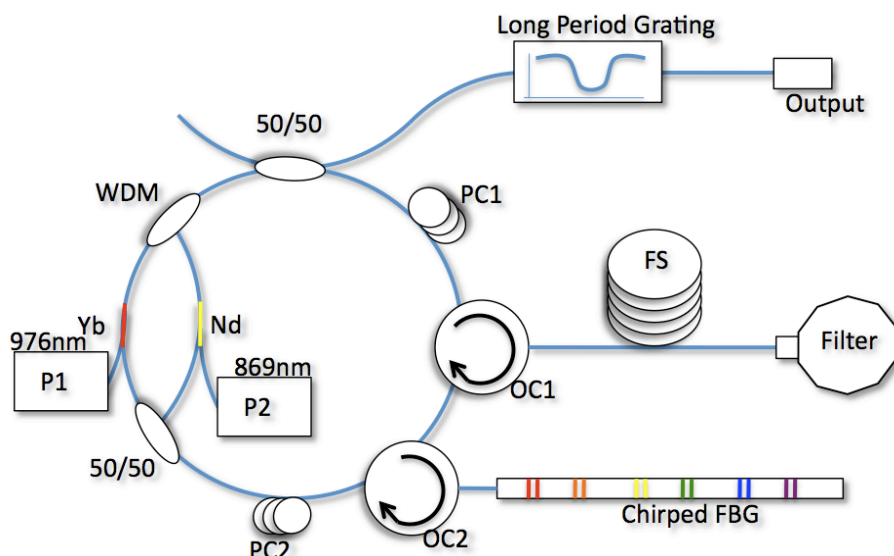


Figure 6-1: Suggested cavity design for an improved spectral FDML response

6.3 Impact to the Field

The greatest impact that this work has on the field, is the output power at 1060nm for swept source OCT. Typical output powers for OCT light sources at this wavelength are all less than 20mW, and this is due to the limitation in the SOA gain medium. 10mW is an adequate amount of output power to image with OCT and have excellent light penetration. With the dual core Yb doped fiber, an output power can be achieved in the wattage range. For the first time, a laser source at 1060nm has an output power greater than 30mW. Because an output power at 200mW is achievable, multi-channeled imaging is now possible as a single light source; it can now provide enough power for several OCT sample arms. An MOCT imaging system centered at the 1060nm water absorption/scattering window impacts the medical imaging field, as there now exists a source that can image multiple regions of the same tissue. More over, this provides the backbone work for the next generation of MOCT systems. Next steps would include catheterization of the multi-channeled source and to perform in-vivo endoscopic imaging to help with either image-guided surgery or for pathology.

7 Bibliography

- [1] W Drexler, "Ultrahigh-resolution optical coherence tomography," *Journal of Biomedical Optics*, vol. 9, no. 1, pp. 47-74, Jan/Feb 2004.
- [2] J. G. Fujimoto, "Optical Coherence Tomography: Introduction," in *Handbook of Optical Coherence Tomography*, G.J. Tearney B.E. Bouma, Ed. New York, NY, USA: Marcel Dekker, 2002, pp. 1-40.
- [3] James G. Fujimoto Wolfgang Drexler, "State-of-the-art retinal optical coherence tomography," *Progress in Retinal and Eye Research*, vol. 27, pp. 45-88, 2008.
- [4] J. Tearney, Mark E. Brezinski, Brett E. Bouma, Stephen A. Boppart, Costas Pitris, James F. Southern, James G. Fujimoto Guillermo, "In Vivo Endoscopic Optical Biopsy with Optical Coherence Tomography," *Science*, vol. 276, no. 5321, pp. 2037-2039, 1997.
- [5] K.K.C Lee, A. Mariampillai, N.R. Munce, M.K.K. Leung, V.X.D. Yang, I.A. Vitkin B.A. Standish, "In vivo endoscopic multi-beam optical coherence tomography," *Phys. Med. Biol.*, vol. 55, pp. 615-622, 2010.
- [6] Woonggyu Jung, Yeh-Chan Ahn, Ali Sepehr, William B. Armstrong, Matt Brenner, Daniel T. McCormick, Norma C. Tien Zhongping Chen, "High speed three-dimensional endoscopic OCT using MEMS technology," in *Proc. of SPIE*, vol. 6466, 2007.
- [7] Jr., MD, Kenji Kobayashi, MD, Joseph A. Izatt, PhD, Andrew M. Rollins, R. Ungrunyawee, AmitabhChak, MD, Richard C.K.Wong, MD, Gerard A.Isenberg, MD, Joseph Willis, MD Michael V. Sivak, "High-resolution endoscopic imaging of GI tract using optical coherence tomography," *GASTROINTESTINAL ENDOSCOPY*, vol. 51, no. 4, pp. 474-479, 2000.
- [8] G.J. Tearney et al., "Endoscopic optical coherence tomography," *Lasers and Electro-Optics Society Annual Meeting*, vol. 1, pp. 328-329, Nov 1996.
- [9] A. Mariampillai, B.A. Standish, K.K.C. Lee, N.R. Munce, I.A. Vitkin, V.X.D. Yang M.K.K. Leung, "High-power wavelength-swept laser in Littman telescope-less polygon filter and dual-amplifier configuration for multichannel optical coherence tomography," *Optics Letters*, vol. 34, no. 18, pp. 2814-2816, Sep. 2009.

- [10] M. Esmaeelpour, B. Povazay, B. Hofer, N. Sheen, R. North, W. Drexler B. Hermann, "Wide field visualization of retinal and choroidal microstructure in vivo frequency domain OCT at 1060 nm with upto 47000 lines/s," in *Proceedings of SPIE 7163*, art. no. 71630A.
- [11] B. Povazay, B. Hermann, H. Sattmann, A. Chavez-Pirson, W. Drexler A. Unterhuber, "In vivo retinal optical coherence tomography at 1040 nm - enhanced penetration into the choroid," *OPTICS EXPRESS*, vol. 13, no. 9, pp. 3252-3258, May 2005.
- [12] J.G. Fujimoto, "Optical coherence tomography," *Applied Physics*, vol. 2, no. 4, pp. 1099-1111, July 2001.
- [13] W. Drexler, C. K. Hitzenberger, T. Lasser A.F. Fercher, "Optical Coherence Tomography - Principles and Applications," *Rep. Prog. Phys.*, vol. 66, pp. 239-303, 2003.
- [14] A. Mauro, "High Speed Rotary System for Catheter Based 3-D Imaging with Optical Coherence Tomography (OCT)," Biomedical Physics, Ryerson University, Toronto, MSc Thesis 2009.
- [15] O. Svelto, *Principles of Lasers*, D. C. Hanna, Ed. New York, United States: Springer, 1998.
- [16] J. Nilsson, A.C. Tropper, D.C. Hanna R. Paschotta, "Ytterbium-doped fiber amplifiers," *IEEE Journal of Quantum Electronics*, vol. 33, no. 7, pp. 1049-1056, Jul 1997.
- [17] A. Mariampillai, B. Vuong, K.H.Y. Cheng, L.R. Chen, X. Gu, B.A. Standish, V.X.D. Yang M.K. Harduar, "Dual core ytterbium doped fiber ring laser in Fourier domain mode locked operation for swept-source optical coherence tomography," in *Proc. SPIE 7580*, 2010.
- [18] M. Wojtkowski, J. G. Fujimoto R. Huber, "Fourier Domain Mode Locking (FDML): A new laser operating regime and applications for optical coherence tomography," *Optics Express*, vol. 14, no. 8, pp. 3225-3237, April 2006.
- [19] Jae Seok Park, Myung Yung Jeong, Chang-Seok Kim, Tae Joong Eom, Cheol-Sik Kee, Do-Kyeong Ko. Eun Joo Jung, "Sweeping Detector OCT based on Fabry-Perot Tunable Filter and Balanced Photoreceiver," *Lasers and Electro-Optic*, Aug 2007.
- [20] D.C. Adler, J.G. Fujimoto R. Huber, "Buffered Fourier domain mode locking: unidirectional swept laser sources for optical coherence tomography imaging at 370,000 lines / s," *Optics Letters*, vol. 31, no. 20, pp. 2975-2977, Oct. 2006.

- [21] S. M. R. Motaghian Nezam, "High-speed polygon-scanner-based wavelength-swept laser source in the telescope-less configurations with application in optical coherence tomography," *Optics Letters*, vol. 33, no. 15, pp. 1741-1743, Aug 2008.
- [22] S.O. Kasap, *Optoelectronics and Photonics Principles and Practices*. Upper Saddle River, NJ: Prentice Hall, 2001.
- [23] M.L. Gordon, B. Qi, J. Pekar, S. Lo, E. Seng-Yue, A. Mok, B.C. Wilson, I.A. Vitkin V.X.D. Yang, "High speed, wide velocity dynamic range Doppler optical coherence tomography (Part I): System design, signal processing, and performance," *Optics Express*, vol. 11, no. 7, pp. 794-809, Apr 2003.
- [24] R. Herda, S. Kivisto, O.G. Okhotnikov M. Rusu, "Fiber taper for dispersion management in a mode-locked ytterbium fiber laser," *Optics Letters*, vol. 31, no. 15, pp. 2257-2259, 2006.
- [25] C. Boudoux, G.J. Tearney, B.E. Bouma S.H. Yun, "High Speed wavelength-swept semiconductor laser with a polygon-scanner-based wavelength filter," *Optics Letters*, vol. 28, no. 20, pp. 1981-1983, 2003.
- [26] J. Zhang, Q. Wang, Z. Chen M.Y. Jeon, "High-speed and wide bandwidth Fourier domain mode-locked wavelength swept laser with multiple SOAs," *Optics Express*, vol. 16, no. 4, pp. 2547-2554, 2008.
- [27] R.M. Percival, I.R. Perry, R.G. Smart, P.J. Suni and A.C. Tropper D.C. Hanna, "An ytterbium-doped fibre laser: broadly tunable operation from 1010 μ m and three-level operation at 974nm," *Journal of Modern Optics*, vol. 37, no. 4, pp. 517-525, 1990.
- [28] N. R. Munce, K. J. Anderson, A. S. Thind, G. Leung, P. E. Radau, F. S. Foster, I. A. Vitkin, R. S. Schwartz, A. J. Dick, G. A. Wright, B.H. Strauss B. K. Courtney, "Innovations in imaging for chronic total occlusions: a glimpse into the future of angiography's blind-spot," *European heart journal*, vol. 29, no. 5, 2008.
- [29] M.L. Gordong, B. Qi, J. Pekar, S. Lo, E. Seng-Yue, A. Mok, B.C. Wilson, A. Vitkin V.X.D. Yang, "High speed wide velocity dynamic range Doppler optical coherence tomography (Part I): System design, signal processing, and performance," *Optics Express*, vol. 11, pp. 794-809, 2003.
- [30] M.D. Duncan, L. Goldberg, J.P. Koplou, J.Reintjes M. Bashkansky, "Characteristics of a Yb-doped superfluorescent fiber source for use in optical coherence tomography," *Optics Express*, vol. 3, no. 8, pp. 305-311, 1998.
- [31] Standish B, Randall C, Liu G, Munce NR, Vitkin IA, Cable A, Jiang J, Yang VXD Mariamplillai A, "Optical Cardiogram Gated 2D Doppler Flow Imaging at 1000 fps and 4D Imaging at 36 fps on a Swept Source OCT System," vol. 15, pp. 1627-1638,

2007.

- [32] Mariampillai A, Standish B, Pop M, Anderson K, Liu G, Luk T, Courtney B, Wright G, Vitkin IA, Yang VXD Munce NR, "Electrostatic Forward-Viewing Scanning Probe for Doppler Optical Coherence Tomography using a Dissipative Polymer Catheter," *Optics Letters*, vol. 33, p. 657, 2008.
- [33] Lee K, Jin X, Mariampillai A, Munce NR, Wood M, Wilson BC, Vitkin IA, Yang VXD Standish BA, "Interstitial Doppler Optical Coherence Tomography as a Local Tumor Necrosis Predictor in Photodynamic Therapy: An in vivo study," *Cancer Research*, vol. 68, pp. 9987-9995, 2008.
- [34] Wright GA, Mariampillai A, Standish BA, Leung KKM, Tan L, Lee K, Courtney BK, Teitelbaum AA, Strauss BH, Vitkin IA, Yang VXD Munce NR, "Doppler optical coherence tomography for interventional cardiovascular guidance: in-vivo feasibility and forward-viewing probe flow phantom demonstration," *Journal of Biomedical Optics*, vol. 15, no. 01, p. 1103, 2010.